RSC Advances

REVIEW

View Article Online
View Journal | View Issue

Cite this: *RSC Adv.*, 2025, **15**, 33773

Biomedical potentials of MXene-based self-powered wearable devices: the future of next-generation wearables

Yeganeh Mohammadi Shahandashti, [a] Sepehr Larijani, [a] Mahnaz Eskandari, *[a] Atefeh Zarepour,[bc] Arezoo Khosravi,[de] Siavash Iravani *[f] and Ali Zarrabi *[g]

MXene-based self-powered wearable devices have emerged as a groundbreaking innovation in the biomedical field, offering significant advancements in health monitoring, disease diagnosis, and therapeutic interventions. This review delves into the unique properties of MXene-based composites, including their excellent electrical conductivity, high mechanical strength, tunable surface chemistry, promising biocompatibility and biodegradability, antibacterial activity, photothermal properties, electrochemical activity, and enzyme-mimicking capabilities, which render them ideal candidates for powering advanced biosensors and other wearable technologies. By capturing energy from body movements or thermal gradients, these devices can operate autonomously, eliminating reliance on external power sources and enhancing user convenience. The integration of MXenes into biosensing applications allows for the continuous and non-invasive monitoring of vital signs and biomarkers, facilitating early detection of diseases such as cancer and diabetes. Additionally, the potential for localized therapeutic applications, such as photothermal therapy, positions MXene-based devices as versatile tools in personalized medicine. Herein, we aim to critically examine the biomedical potentials of MXene-based self-powered wearable devices, focusing on their applications in health monitoring, disease diagnosis, and therapeutic interventions. Additionally, this review focuses on the challenges confronting MXene-based self-powered wearable devices, while also exploring future perspectives and innovations that could enhance their performance and applicability in biomedical fields.

Received 28th June 2025
Accepted 29th August 2025

DOI: 10.1039/d5ra04611d

rsc.li/rsc-advances

1 Introduction

Self-powered wearable devices are advancing the biomedical field by enabling continuous, non-invasive health monitoring without relying on external power sources.[1,2] These innovative technologies capture energy from various environmental sources, including mechanical movements, body heat, and biochemical reactions, to power sensors and electronic components.[2–5] Key energy harvesting technologies include triboelectric nanogenerators (TENGs), which convert mechanical energy into electricity, piezoelectric nanogenerators (PENGs) that generate electricity from mechanical deformations, thermoelectric generators (TEGs) that utilize body heat, and biofuel cells that convert biochemical energy from body fluids.[6,7] Together, these technologies enhance the functionality and independence of wearable devices, allowing for continuous monitoring of vital signs and early disease detection. Despite their promising potential, self-powered wearables face challenges such as improving energy harvesting efficiency, ensuring long-term stability, and developing multimodal sensing capabilities. Research is underway to address these issues, focusing on advanced materials, flexible designs, and hybrid energy harvesting systems to enhance efficiency and versatility. Recent advances also include perspiration-powered electronics, which utilize human sweat for energy generation, showing promise for metabolic sensing applications. As these technologies continue to evolve, self-powered wearable devices are poised to play a transformative role in personalized medicine, health monitoring, and therapeutic applications, ultimately improving health outcomes and user convenience.[8]

[a]*Department of Biomedical Engineering, Amirkabir University of Technology, Tehran, Iran. E-mail: eskandarim@aut.ac.ir*

[b]*Department of Biology, Faculty of Arts and Sciences, Kocaeli University, İzmit, Kocaeli , 41001, Türkiye*

[c]*Department of Research Analytics, Saveetha Dental College and Hospitals, Saveetha Institute of Medical and Technical Sciences, Saveetha University, Chennai-600077, India*

[d]*Department of Genetics and Bioengineering, Faculty of Engineering and Natural Sciences, Istanbul Okan University, Istanbul 34959, Türkiye*

[e]*Graduate School of Biotechnology and Bioengineering, Yuan Ze University, Taoyuan 320315, Taiwan*

[f]*Independent Researcher, W Nazar ST, Boostan Ave, Isfahan, Iran. E-mail: siavashira@gmail.com*

[g]*Department of Biomedical Engineering, Faculty of Engineering and Natural Sciences, Istinye University, Istanbul 34396, Türkiye. E-mail: alizarrabi@gmail.com*

MXenes, a class of two-dimensional (2D) transition metal carbides and nitrides, have emerged as promising materials for self-powered wearable devices due to their exceptional electrical conductivity, large surface area, and tunable interfacial properties.[9,10] These characteristics make MXenes ideal for applications in energy storage and harvesting, which are crucial for powering wearable electronics without external power sources. Their potential in the biomedical field is particularly noteworthy, as MXene-based wearable devices can facilitate health monitoring, disease diagnosis, and therapeutic interventions.[11,12] For instance, flexible epidermic sensors made from antibacterial MXene hydrogels show great promise in personalized healthcare and human–machine interfaces, as they combine self-healing capabilities, high-performance sensing, and accelerated wound healing for multifunctional applications.[13] With biocompatibility and low cytotoxicity, MXenes are suitable for use in wearable biosensors, enabling real-time physiological monitoring through mediator-free biosensors and enhancing comfort through flexible and stretchable designs. The performance of MXenes in wearable devices can be significantly enhanced through multi-interface engineering, which includes surface modification and interfacial manipulation. Integrating MXenes with other materials leads to composite structures that improve energy harvesting efficiency and sensing capabilities.[14–16] However, challenges remain, such as enhancing long-term stability and developing sophisticated sensing modalities. Future studies will likely focus on optimizing these multi-interface techniques and exploring new composite materials while integrating MXene-based devices with emerging technologies like artificial intelligence (AI) and the internet of things (IoT).

The ability to power devices without external energy sources is particularly advantageous in healthcare settings, where continuous monitoring and real-time data analysis are crucial for effective patient management.[17,18] MXene-based self-powered devices excel in health monitoring and diagnostics due to their ability to integrate energy harvesting mechanisms, such as TENGs and PENGs.[19] These devices can convert mechanical energy generated from body movements into electrical energy, powering sensors that continuously monitor vital signs, such as heart rate, blood pressure, and glucose levels. Additionally, MXenes can be utilized in biosensors for detecting specific biomarkers, enabling early disease diagnosis. Their mediator-free biosensors facilitate direct electron transfer between bioreceptors and electrodes, allowing for real-time physiological data collection and analysis. Beyond monitoring, MXene-based self-powered devices hold potential for therapeutic applications. For instance, they can be integrated into implantable devices for electrical stimulation, promoting tissue regeneration and healing in conditions such as osteoporosis or nerve damage. Additionally, the versatility of MXenes allows for the development of flexible and stretchable systems that conform to the body's contours, enhancing patient comfort and compliance.[19]

The purpose of this review is to explore the biomedical potentials of MXene-based self-powered wearable devices, highlighting their innovative applications in health monitoring, disease diagnosis, and therapeutic interventions. First, the mechanisms of energy harvesting are discussed. By examining the unique properties of MXenes and their composites, such as their exceptional electrical conductivity, biocompatibility, and adaptability, this review aims to showcase how these materials can be integrated into wearable technologies to enhance continuous physiological monitoring and improve patient outcomes. Additionally, it addresses the challenges and future directions in optimizing MXene-based self-powered wearable devices, including device design and fabrication, energy harvesting efficiency, and long-term stability, to fully realize their transformative impact on personalized medicine and healthcare solutions.

2 Mechanisms of energy harvesting

2.1 Source of human body energy

The human body metabolizes nutrients to generate energy, which is utilized for maintaining thermoregulation and sustaining physiological functions, while surplus energy is dissipated into the surrounding environment. The generated energy can be classified into thermal, chemical, and mechanical forms. Advanced energy-harvesting strategies aim to capture these physiological energy sources and convert them into electrical power, thereby enabling the operation of self-powered wearable devices.[20]

2.1.1 Mechanical energy. Mechanical energy is one of the most prevalent forms of energy encountered in daily life. It arises from various bodily motions, including limb movements (*e.g.*, foot lifting, stepping, arm raising, tapping, and knocking) as well as physiological activities such as heartbeat and respiration, which contribute to continuous mechanical energy cycles. This energy originates from the contraction and relaxation of muscles during internal physiological processes, subsequently generating external mechanical forces. Such biomechanical activities produce localized mechanical energy that can theoretically be harvested to power wearable or implantable biomedical devices. Recent studies have demonstrated the potential of MXene-based wearable systems in this area, highlighting their remarkable piezoelectric and triboelectric properties for efficient harvesting of mechanical energy.[21,22] MXene-based sensors monitor physiological functions (swallowing, coughing), joint movements (elbow, fingers, ankle), and subtle micro-expressions (eye blinking, cheek bulging, throat swallowing).[23]

2.1.2 Thermal energy. Recent advancements in MXene-based technologies have demonstrated considerable potential for harvesting mechanical energy from various bodily motions. However, the generation of mechanical energy is highly dependent on human activity and movement patterns. To complement this, the human body also serves as a reliable source of thermal energy, which is continuously produced through basal metabolic processes. This constant heat generation can be effectively harvested using thermoelectric and pyroelectric devices to power wearable sensors. Following food intake, energy is stored primarily as glycogen or fat, while the remaining portion is converted into adenosine triphosphate

(ATP), which fuels essential cellular processes such as movement, cognition, and respiration. In this context, the human body functions as a continuous energy-generating system. Dissipative processes such as respiration and heat loss through sweating represent key routes of energy release, which can be harnessed as potential power sources for wearable devices.[20]

2.1.3 Biofluids and biochemical reactions. Biochemical wearable devices play a crucial role in collecting and monitoring biomarkers from biofluids such as sweat, saliva, and interstitial fluid (ISF). These biomarkers reflect physiological status and disease progression, making their continuous monitoring essential for early diagnosis and personalized healthcare.[20,24] Sweat is one of the most widely studied non-invasive fluids, containing electrolytes (Na^+, K^+, Cl^-), metabolites (glucose, lactate, urea, creatinine), and trace nutrients that provide valuable insights into cardiovascular function, metabolic activity, and nutritional balance. For instance, sweat glucose monitoring offers a promising alternative to finger-prick tests in diabetes detection, while electrolyte imbalance can indicate neuromuscular disorders and dehydration. Among these, lactate produced during anaerobic metabolism is a key marker for muscle activity and fatigue. Importantly, MXene-based sensors have demonstrated high accuracy and stability in tracking sweat glucose and electrolyte levels in real time.[25,26] Interstitial fluid (ISF), the primary extracellular fluid in the body, diffuses directly from the bloodstream and often provides more accurate information than sweat. ISF analysis enables real-time monitoring of glucose, electrolytes, pH, and cytokines, making it valuable for the early detection of diabetes, cardiovascular disorders, and certain cancers.[26,27] Saliva, the most easily accessible biofluid, contains diverse biomarkers such as electrolytes, hormones, and metabolites that mirror systemic health. However, its clinical application faces challenges due to low analyte concentrations and the complexity of its composition. Uric acid (UA) is a particularly important salivary biomarker, as abnormal levels are associated with hyperuricemia, gout, and kidney dysfunction.[26] Beyond biomarker detection, MXenes also enable energy harvesting to power wearable devices. Their high surface reactivity and tunable chemistry allow efficient interactions with enzymes, proteins, antibodies, and small molecules, significantly improving biosensor selectivity and sensitivity. For example, antibody-functionalized MXene surfaces have shown enhanced detection of tumor markers.[28,29] Moreover, body fluids can serve as natural fuel sources in biofuel cells (BFCs), which convert chemical energy from glucose or lactate into electricity. This non-invasive power generation strategy makes BFCs highly attractive for self-sustaining wearable systems. Finally, energy-harvesting technologies for wearable healthcare devices are generally classified according to their source: mechanical energy (piezoelectric nanogenerators, PENG; triboelectric nanogenerators, TENG), thermal energy (thermoelectric generators, TEG; pyroelectric generators, PEG), and biochemical energy (BFCs). While only a fraction of physiological energy can be harvested safely, the integration of MXene-based materials into these systems offers new opportunities for efficient, multifunctional, and self-powered wearable platforms.[30]

2.2 Mechanisms of self-powered wearable devices

Recently, capturing energy from the human body, derived through metabolic conversion of nutrients, and expanded heat and body movement has emerged as a promising clean energy source. The most important forms of energy, including thermal, chemical, and mechanical energy, can be converted into electrical energy. Nevertheless, developments in human energy harvesting faced significant challenges like disruption of body functions, low conversion efficiency, and limitations in usable energy output. However, this microwatt to milliwatt energy is promising for powering low-power devices like wearables and medical implants.[31] Indeed, traditional batteries, with their limited capacity and need for frequent recharging, are insufficient to meet the requirements of modern wearable electronics. A self-powered nanosystem comprises a sensor, data processing, and an energy harvesting and storage device. The energy harvester is designed to convert different forms of energy, such as mechanical, thermal, and chemical energy, into electrical voltage. The harvested energy sustains all stages of the sensing process, including collecting data, processing, and transmission.[32] In this context, MXenes, with their two-dimensional structure, high specific surface area, metallic conductivity, mechanical stability, and hydrophilicity, have garnered significant attention as materials for energy-harvesting applications.[33] There are five different types of energy harvesting methods based on their source: a photovoltaic harvester that converts sunlight into electricity, which is used in lights and charging stations. Piezoelectric transforms stress and vibration into electrical power, showing potential in sensors and monitoring devices. Electrodynamic harvesters convert magnetic field changes and motion energy into electricity, as in wind turbines and generators. Thermoelectric generators convert body temperature differences into electrical power, which is used to recycle wasted heat.[6]

2.3 Energy harvesting from biomechanical movements

Body movements, including walking, foot lifting, heartbeat, and even contraction of blood vessels, are associated with the release of energy. Biomechanical energy harvesting from human body movements is an independent and reliable method for providing continuous power.[7] Nanogenerators can harvest from large movements to small activities, such as a heartbeat, and contractions, to provide renewable energy for wearable devices.[8]

Flexible wearable sensors can be categorized into two types. The first type relies on conventional semiconductor processes, in which conductive wires connect the sensing components to the body to form functional sensors. The second type utilizes advanced triboelectric and piezoelectric materials, which enable the sensors to exhibit substantial stretchability and flexibility and convert these mechanical forces to electrical energy. Since traditional semiconductor sensors tend to be rigid, they face challenges in small-sized and wearable devices. In contrast, modern approaches involving ductile sensor devices-composed of carbon, metal, and conductive materials-offer enhanced adaptability and performance. An ideal sensor

should offer flexibility, high sensitivity, a wide detection range, low detection limits, and fast response. Among these factors, sensitivity and detection range are the most crucial in determining overall effectiveness.[34] Due to their excellent mechanical and thermal properties, biomechanical sensors have been developed using conductive polymers, graphene, and carbon nanotubes. However, their applications have been limited by the complex and expensive fabrication methods required for high-sensitivity sensors. Factors such as cost, hypoallergenic properties, and sustainability must also be considered. Although the current production cost of $Ti_3C_2T_x$ MXene is generally higher than that of graphene, its superior oxidation resistance, tunable surface chemistry, and high electrical conductivity can enhance device durability and long-term stability in wearable applications. These advantages may offset the initial expense, making MXenes a promising alternative for wearable pressure sensors.[35]

TENGs are self-powered energy sources that convert daily mechanical energy from human motion into electrical energy. With numerous advantages based on the materials that are used in their structure, such as low cost, optimized surface efficiency, humidity-proof, lightweight design, and biocompatibility, TENGs have become highly attractive for use in wearable and portable devices.[1] They work by combining electrostatic induction and polarization. When two dielectric materials come into contact, they generate opposite charges on their surfaces. Moreover, mechanical motion makes a potential difference across electrodes, driving electron flow (Fig. 1A).[9] When atoms are far from each other, their electron clouds are isolated, which prevents electrons from having the energy to pass the transfer barrier. But an external force pushes the atoms closer, so their electron clouds begin to overlap (Fig. 1C). This overlap allows electrons to gain enough energy to transfer between atoms. Based on this theory, TENG has different working modes (Fig. 1B). The vertical contact-separation mode has a simple structure and immediate power generation. In the lateral sliding mode, movements generate energy that generally has a higher output voltage and current. In smart wearable applications where TENG components are often dynamic and hard to wire, the single-electrode mode with one grounded electrode is an excellent choice for self-powered sensing devices. In the freestanding mode, a pair of symmetric electrodes is used instead of a ground reference to achieve high outputs through asymmetric charge distribution during free movement. Additionally, the rolling mode contains small balls on the layer to facilitate charge transfer between electrodes. This idea reduces material abrasion during higher output.[36]

One of the important points that should be considered for the fabrication of TENGs is the choose of materials that could improve their properties. Polytetrafluoroethylene (PTFE) is one of the electron acceptor materials widely used in TENGs to achieve significant potential differences, which have interesting

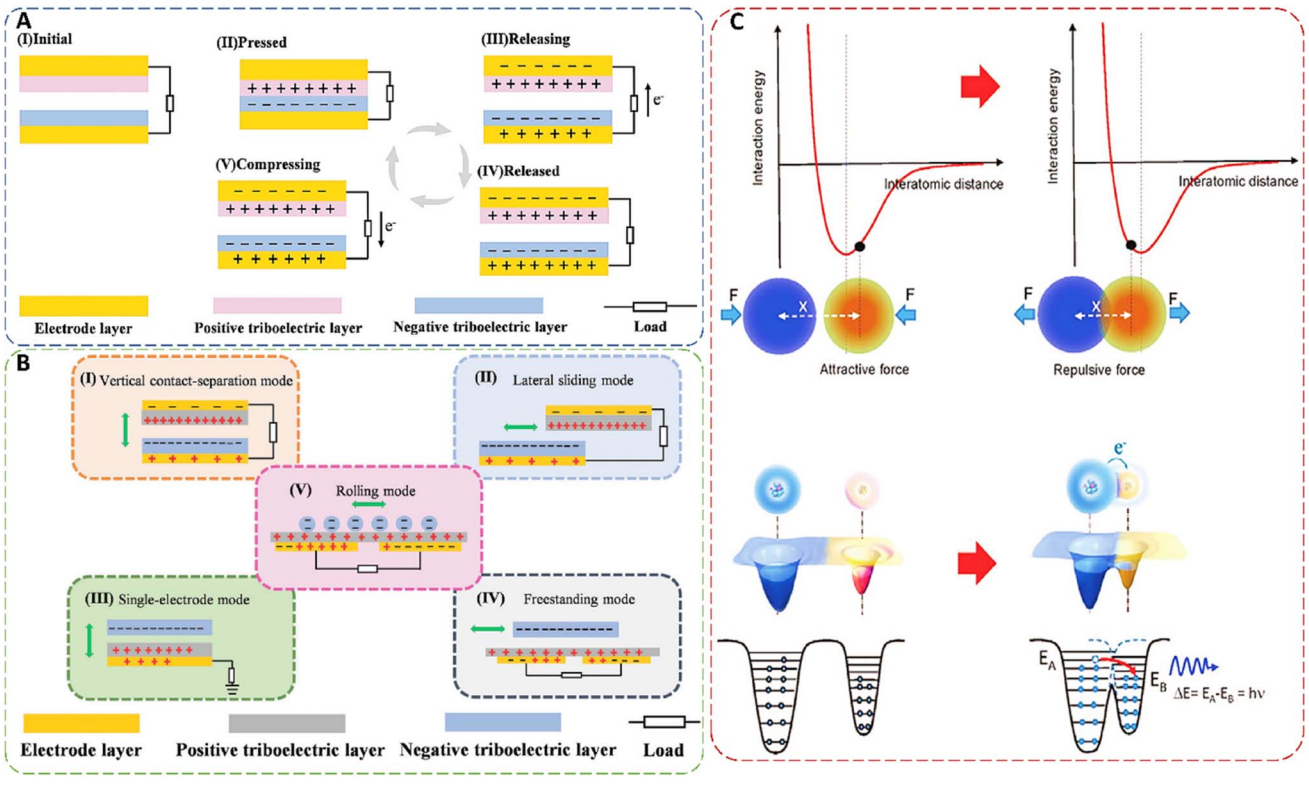

Fig. 1 (A) The mechanism of TENG's working, including (I) initial, (II) pressed, (III) releasing, (IV) released, and (V) compressing. (B) Five basic modes of TENGs: (I) vertical contact-separation mode. (II) Lateral sliding mode. (III) Single-electron mode. (IV) Freestanding mode. (V) Rolling mode. (C) Explaining the contact electrification (CE) model and how charge transfers between two atoms. Reprinted with permission from ref. 37. Copyright 2024, Wiley-VCH GmbH.

properties, including low friction, a low dielectric constant, high mechanical strength, and excellent plasticity. Due to the electrically insulating nature of PTFE-based TENGs and their heat and chemical resistance, it is challenging to design conductive PTFE or apply metallic coatings to their surface. Similar difficulties have remained in polymers like polydimethylsiloxane (PDMS) and fluorinated ethylene propylene (FEP).[38] Two-dimensional MXene with an electronegative surface provides a solution to limitations such as low voltage, poor conductivity, and negligible compared to electronegative polymers (PTFE, PDMS, and FEP).[39]

Luo *et al.* presented a flexible TENG fabricated *via* utilizing MXene/polyvinyl alcohol (PVA) hydrogel (MH-TENG) for energy harvesting and self-powered sensors. The fabricated sensor generated a short-circuit current of 1.2 μA, an open-circuit voltage of 180 V, and a charge transfer of 32 nC. Excellent stretchability enabled it to detect wrist, elbow, and finger movements in real-time and convert bending angles (30°, 45°, 60°, 90°) into voltage signals. Additionally, Ecoflex® encapsulation ensured durability, stability, and environmental friendliness for wearable applications. The MH-TENG is highly stretchable and sensitive to body movements, making it perfect for wearable motion monitoring.[40]

A multifunctional and stretchable double-layered TENG was fabricated in a research study using a nanoporous cobalt oxide (NPCO)/silicone and MXene/silicone nanocomposite. The nanocomposite-based double-layered triboelectric nanogenerator (NDL-TENG) had a high surface area and negatively charged NPCO oxygen, increasing the surface density. Utilizing MXene improved charge trapping and optimized the output voltage. The maximum power density was 10.4 W m^{-2} which was 23 times higher than pure silicone-based TENG. The output voltage, current density, and sensitivity were 1680 V, 560 mA m^{-2}, and 5.82 V kPa^{-1}, respectively. The NDL-TENG effectively recorded motion from finger bending (30–90°), wrist flexion (30–90°), elbow (30–120°), and knee movement (30–90°). After 50 000 mechanical cycles, the output remained stable and suitable for real-time physiological monitoring, demonstrating excellent durability for the long term.[41]

Jiang *et al.* Constructed a high-performance MXene–PDMS composite film integrated with a laser-induced graphene (LIG) electrode.[42] This design achieved a 7-fold increase in output performance compared to conventional PDMS-based TENGs. The TENG demonstrated a peak output voltage of 119 V, a current of 11 μA, and an optimized power density of 609.1 mW m^{-2} at a load resistance of 8 MΩ, powering 522 light-emitting diodes (LEDs) in series. The device harvested leaf swing energy and generated a voltage in response to wind speeds from 1 to 5 m s^{-1}, with output increasing from 0.5 V to 2.0 V. The sensitivity of MXene-based TENG showed its potential for environmental sensing and wind energy harvesting. The MXene-enhanced PDMS porous film and LIG electrode improved triboelectrification and charge transfer, making the fabricated composite suitable for wearable electronics, self-powered sensors, smart agriculture, robotics, and human–machine interfaces.

Cao *et al.* designed a shape-adaptive TENG enhanced by MXene electrodes as a biomechanical wearable device. In the process, MXene nanosheets were mixed with cellulose nanofibers (CNFs) to form a dispersion, which was injected into a silicone rubber capsule to create the CM-TENG device with specific properties such as high performance under deformation and reliably powers small electronics like LED lights and wearable sensors. The open-circuit voltage (V_{oc}), short-circuit current (I_{sc}), and transferred charge (Q_{sc}) were reported as 300 V, 5.5 μA, and 120 nC. The CM-TENG can be used as a biomechanical sensor by attaching to skin or clothes for real-time monitoring of various human motions.[7]

In another study, He *et al.*,[43] presented a flexible single-electrode TENG of a MXene ($Ti_3C_2T_x$)/PDMS composite film. They investigated the effects of MXene concentration and applied compressive force on the device's performance and revealed its applications as real-time monitoring detection, energy harvesting, and smart textiles. The high conductivity and electronegativity of MXene enhances the electrical output and improves surface charge density. The device successfully detected various human motions, including finger tapping (25 V, 4 μA cm^{-2}), hand clapping (45 V, 7.5 μA cm^{-2}), and hand hammering (42 V, 7 μA cm^{-2}).

PENG generates an electric field in response to mechanical deformations. PENGs are a leading technology for energy harvesting with various applications such as structural monitoring, transportation, wireless electronics, micro-electromechanical systems (MEMS), Internet of Things (IOT), and biomedical devices. Advanced materials such as polyvinylidene fluoride (PVDF), barium titanate (BTO), PTZ (lead zirconate titanate), zinc oxide (ZnO), and nylon have been developed for nanostructures, thin films, and layered stacks to create efficient piezoelectric generators. Piezoelectricity arises from the linear electromechanical interaction in crystals lacking inversion symmetry. Unlike symmetrical metals, piezoelectric crystals experience atomic displacement that disrupts charge balance, generating an electric field. This effect extends across the structure, creating opposite charges on its outer surface. The piezoelectric layer is between two surfaces where charge accumulates. This layer applies electrostatic induction and generates a steady current in response to the piezoelectric field.[44,45]

The efficiency of piezoelectric energy harvesting relates to the direction of the mechanical force. When the applied force and the electrical polarization are on the same axis, the system functions in the d_{33} mode. Conversely, when the applied force is oriented perpendicular to the direction of electrical voltage, the system operates in the d_{31} mode. The overall performance of a PENG is quantitatively determined by the magnitude of the piezoelectric charge coefficient (d_{ij}), where i relates to the polarization direction and j represents the direction of the applied mechanical stress.[45] Fig. 2A shows the atomic structure of Ti_3C_2 MXene monolayers. Three types of colored balls are used to show different atoms: Titanium (Ti) atoms are represented in blue, Carbon (C) atoms in purple, and functional groups (T_x) in green. The piezoelectric responses with an external resistor are studied by applying mechanical strains (Fig. 2B and C). When strain is applied, the structure

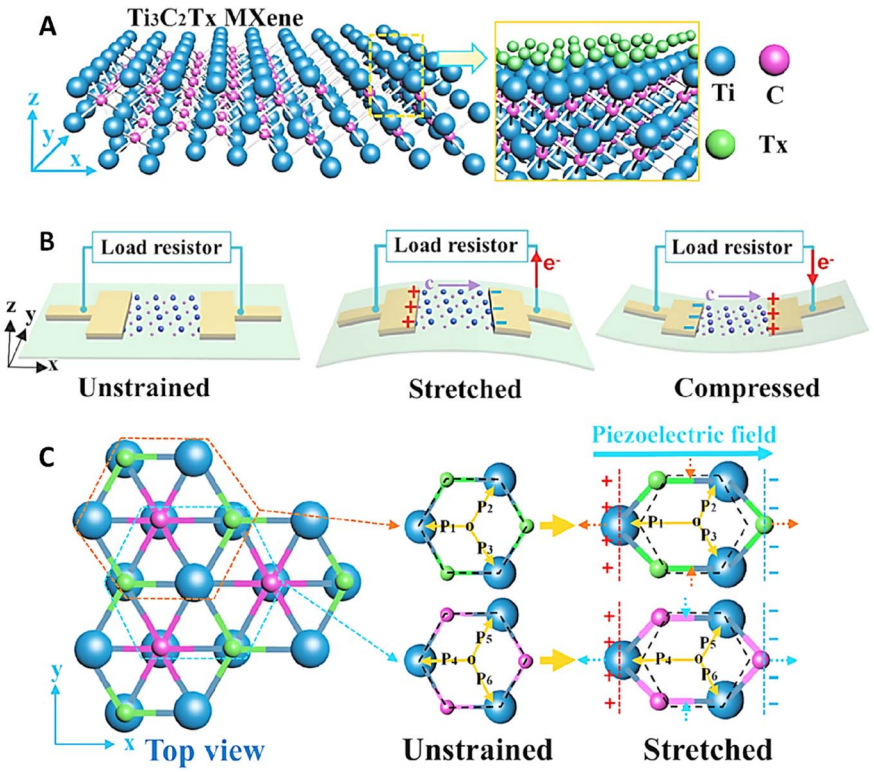

Fig. 2 (A) Atomic structure of the monolayer $Ti_3C_2T_x$-MXene (left) and $Ti_3C_2T_x$-MXene with functional groups of Ti (right). (B) The $Ti_3C_2T_x$-MXene piezoelectric device works by bending a PET substrate outward and inward, creating tensile and compressive strains in the layer. For measuring and recording the signals, electrodes are used to connect the device to an external circuit to measure and record the piezoelectric signals. (C) Top view of the $Ti_3C_2T_x$-MXene monolayer. Reprinted with permission from ref. 46. Copyright 2021, Elsevier Ltd.

experiences deformation, leading to charge polarization that drives electron flow through the external circuit. As the substrate returns to its original state upon release, the electrons flow back in the opposite direction.[46]

Guo *et al.*,[47] developed a flexible and biodegradable transient pressure sensor by incorporating a porous MXene-based tissue paper between polylactic acid (PLA) sheets. This highly sensitive sensor can be attached to human skin to monitor physical forces, such as wrist pulse measurements, and diagnose diseases, including early-stage Parkinson's disease (PD), by detecting low-frequency physiological variations. The MXene/tissue-paper-based pressure sensor exhibited excellent sensitivity and flexibility, making it highly suitable for real-time motion detection and biomedical applications. It demonstrated a low detection limit of 10.2 Pa, the capability to sense sugar granules as light as 2.3 mg, minimal power consumption (10^{-8} W), a rapid response time of less than 11 ms, and excellent durability with reproducibility over 10 000 cycles. Furthermore, electronic skins were successfully fabricated using sensor arrays, enabling the detection of tactile signals and the mapping of spatial pressure distributions.

A sensitive and flexible helical core–shell structure with a MXene layer designed for full-range detection of human activities such as wrist pulse, forearm twisting, finger bending, knee bending, and speaking. This strain sensor exhibited a wide detection range from 0.3–120% strain, with a gauge factor of 0.67, a response time of 120 ms, and durability exceeding 10 000 cycles at 100% strain. The humidity sensing part demonstrated high sensitivity from 30–100% relative humidity, with a linear resistance change on a semi-log scale. Stable performance for over 50 days at 30% relative humidity was reported and validated in different environments, such as shopping malls, laboratories, forests, and riversides. The MXene-based helical sensor offered a promising approach for next-generation wearable electronics for health monitoring and real-time motion detection.[48]

In contrast to piezoelectric and triboelectric self-powered sensors, which produce electrical signals through polarization or electron movement in response to mechanical forces, biological systems generate electrical signals by transporting ions instead of electrons. Therefore, the development of self-powered sensors utilizing ion transport mechanisms is critically important. Piezo-ionic material can directly convert mechanical signals into electricity by ion migration. These wearable sensors are mostly used for healthcare, human motion detection, electronic skin, and medical rehabilitation.[49] Li and his colleagues produced a piezo-ionic sensor based on a composite of MXene and silver (Ag) nanoparticles used as electrode materials (Fig. 3A) for detecting real-time signals, including specific parameters related to cardiopulmonary resuscitation (CPR), such as chest compression rate and rhythm increases the interfacial area, further enhancing the capacity for

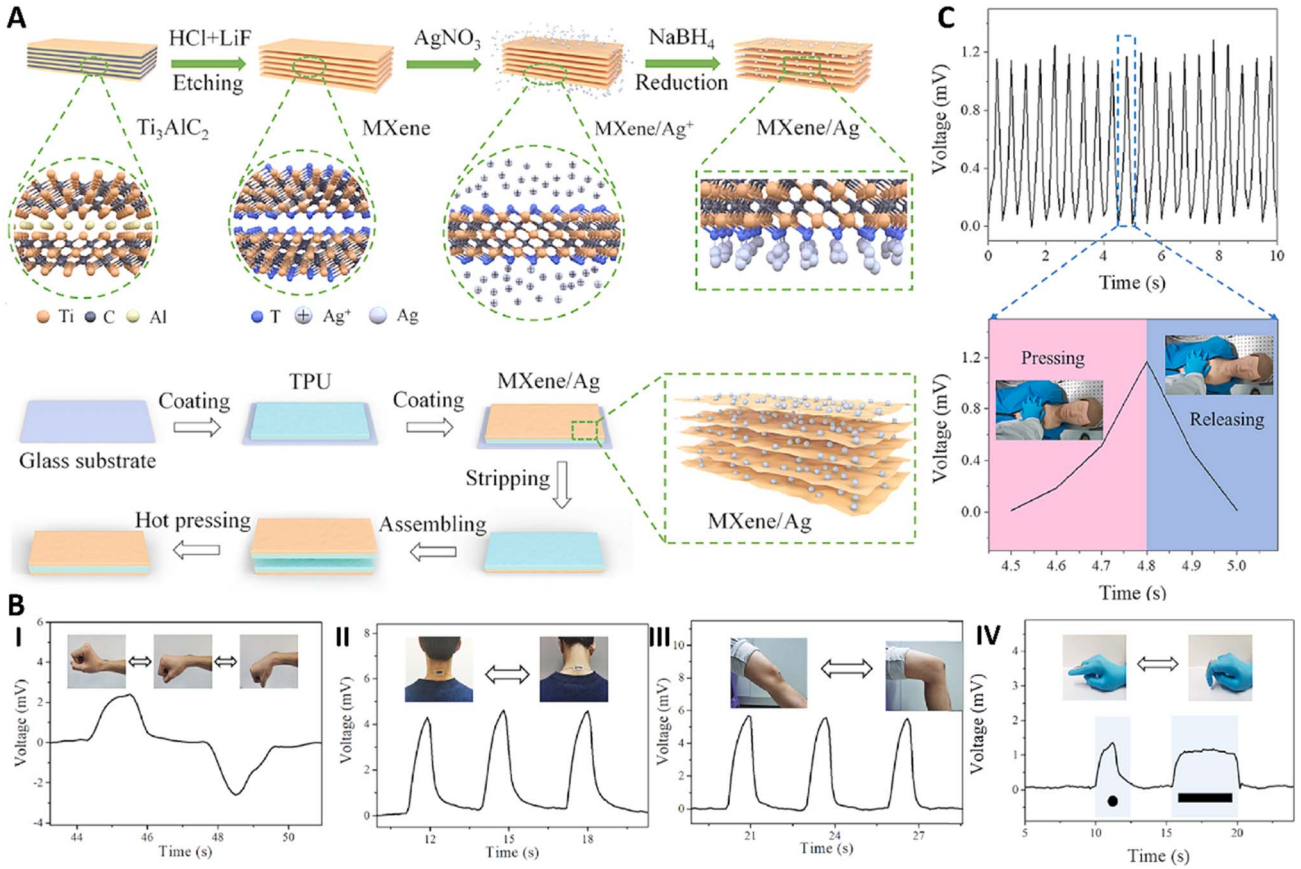

Fig. 3 (A) Schematic of MXene/Ag piezo-ionic sensor fabrication. (B) Sensing signals for monitoring (I) wrist bending, (II) knee, (III) neck movement, and (IV) output voltage–time curve of the sensor for responses to the different bending movements of the finger to record dots and dashes as Morse code. (C) Voltage response to chest compression during CPR. Reprinted with permission from ref. 49. Copyright 2024, Elsevier B.V.

ion accumulation. The resulting sensor exhibited a high voltage output of 11.1 mV under a bending deformation of 0.7% strain and demonstrated outstanding stability, maintaining 95% of its signal over 13 000 seconds of cyclic bending. This wearable sensor was attached to the wrist, neck, elbow, and knee joints to generate electrical signals by detecting body movement (Fig. 3B). The sensor could generate different shapes, such as dots (.) and dashes (/) symbols in Morse code by finger joint replacement. It was also applied on the chest to check the standard gesture of chest compression (Fig. 3C).[49]

2.4 Thermal energy harvesting in wearable applications

The human body expends a substantial amount of thermal energy daily by dissipating it into the environment and through processes such as breathing and sweat evaporation, helping to maintain a normal body temperature.[14] Thermoelectric devices can convert the temperature difference between the human body and its surroundings into electrical energy. The MXene family, with controlled surface functionalization, has been widely explored for thermal energy storage and has demonstrated great potential in flexible and wearable thermoelectric energy-harvesting applications compared to other solution-processed 2D materials.[6,15] The thermal energy harvester methods are the TEG and the PEG. TEGs utilize spatial temperature differences for energy conversion, whereas PEGs rely on temporal temperature variations. As a result, each type of thermal energy harvester is suited for specific applications and forms when capturing thermal energy from the human body.[16]

Thermoelectric energy conversion is defined as converting heat to electricity (Seebeck effect); a temperature-dependent property, that attracts attention to energy-harvesting wearable devices.[17] The thermoelectric voltage changes (ΔV) per unit temperature (ΔT) is defined as the Seebeck coefficient. Seebeck coefficient can be determined *via* eqn (1):[18]

$$S(T) = \frac{dV}{dT} \quad (1)$$

The TEG module contains between 10 to 100 n-type and p-type elements that are electrically connected *via* PbSn or BiSn in series and thermally in parallel and intervene between two ceramic layers. TEG converts thermal energy into electrical energy according to a temperature gradient.[16] The thermo-electrical efficiency of a TEG can be measured by the figure of merit (ZT) as shown in eqn (2):

$$ZT = \frac{S^2 \sigma\, T}{K} \quad (2)$$

where S is the Seebeck coefficient ($\mu V\ K^{-1}$), σ is the electrical conductivity ($\Omega^{-1}\ m^{-1}$), T is the absolute temperature (K), and K is the thermal conductivity ($W\ m^{-1}\ K^{-1}$).[16]

Maintaining a large and constant temperature difference is challenging in the real-world environment. Additionally, thermoelectric devices based on the Seebeck effect still have low efficiency. The pyroelectric nanogenerators with a functional layer of polymer use a different approach that has no Seebeck effect.[18] Cao *et al.*[50] represented a fraction method for highly flexible temperature sensors based on $Ti_3C_2T_x$ incorporated into a PDMS substrate for skin applications. By finely tuning the etching and delamination conditions, they produced MXene nanosheets and lamellae with a hybrid conductive network morphology. TMA-sensors showed a resistance increase of up to 10^4-fold over 25–60 °C, while the HF_{18}-d_2-$Ti_3C_2T_x$ sensor exhibited a 800-fold variation over 25–140 °C, with the HF_6-d_3-$Ti_3C_2T_x$ variant striking an optimal balance. These devices achieved a fast response time of 6.3 s, an outstanding sensitivity of up to 986 °Ca, a wide operational range of 140 °C, an accuracy of 0.1 °C, and great durability over 100 heating cycles. Moreover, this device can detect non-contact temperature by a maximum sensing distance of 9 cm with a minimal resistance variation of 0.01%.

Li *et al.*[51] presented a printable dual-parameter sensor that independently detected strain from temperature variations without crosstalk. The sensor was fabricated using a MXene–silver nanowire (Ag NW)–poly(3,4-ethylenedioxythiophene) polystyrene sulfonate (PEDOT:PSS)–tellurium nanowire (Te NW) nanocomposite that converted strain and temperature to electrical signals through electrical conductivity of MXene (Fig. 4A). The sensor achieved an impressive temperature

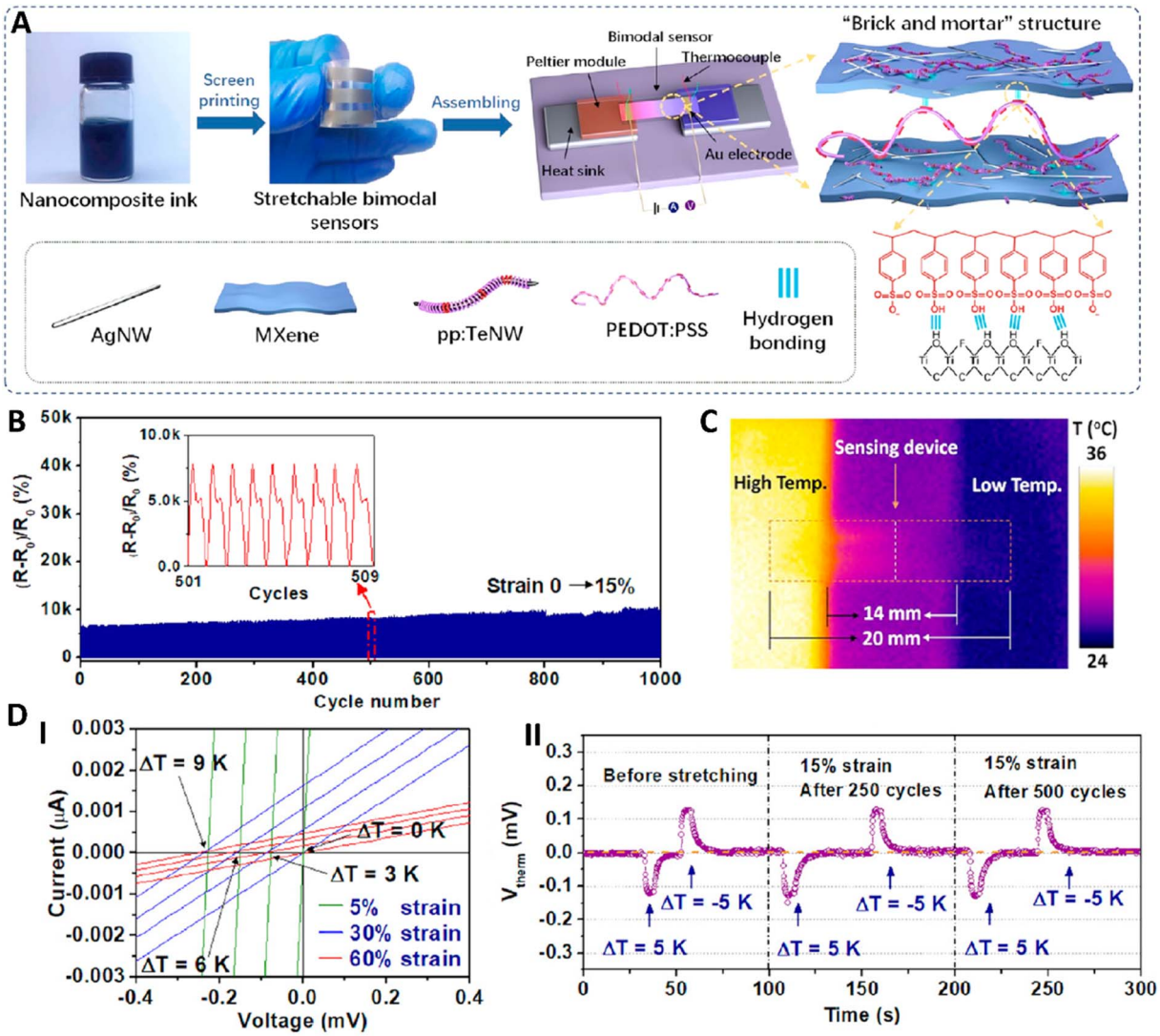

Fig. 4 (A) Schematic image related to the production of MXene–AgNW–PEDOT:PSS–pp:TeNW dual-parameter sensor. (B) Changes in resistance from 0 to 15% strain over 1000 stretching and releasing cycles. (C) Result of the infrared temperature distribution of the sensor. (D) Results of sensing taken using different ΔT (0, 3, 6, and 9 °C) and different strains (5%, 30%, and 60%) (I). Results of heating and cooling cycles in different situations (II). Reprinted with permission from ref. 51. Copyright 2020, American Chemical Society.

resolution of 0.2 °C in an unstretched state and maintained 0.5 °C accuracy at 40% strain. Its strain sensitivity was demonstrated by a gauge factor of up to 1933.3, covering a 62% strain range. The device responded with a heating response time of 1.8 seconds and a relaxation time of 6.5 seconds (Fig. 4C). The MXene–Ag NW conductive network enabled precise strain detection, while the PEDOT:PSS–Te NW hybrid provided thermoelectric temperature sensing, ensuring no signal crosstalk. The sensor exhibited excellent durability, maintaining stable performance after 500 stretching cycles (Fig. 4D) and sustaining accurate detection even after 1000 strain cycles at 15% strain (Fig. 4B).

A PEG is a type of thermal energy harvester that occurs in crystals with a spontaneous polarization property. When the temperature of these crystals varies, the strength of their spontaneous polarization also changes, potentially leading to the formation of surface polarization charges in a particular direction. The pyroelectric has two effects including first-order and second-order. The first-order pyroelectric effect is present in ferroelectric materials like PZT and BTO ceramics, and it involves the generation of charges without any strain. The electric dipoles oscillate randomly at room temperature, while maintaining an average spontaneous polarization, resulting in no electron flow. With rising temperature, the oscillation of the dipoles becomes more intense, increasing their angle of oscillation. This increase reduces the total average spontaneous polarization, decreasing the induced charge on the electrodes and causing electron flow. Conversely, when the temperature drops, the oscillation angles decrease due to reduced thermal energy. This reduction increases spontaneous polarization, leading to a higher induced charge and electron flow in the opposite direction.[14]

3 MXene-based self-powered wearables: design and sensing materials

3.1 Common 2D materials for biosensing

Wearable devices are commonly used to detect human motion or analytes (*e.g.*, ions and molecules) in body fluids by monitoring changes in their electrical signals. Therefore, the sensing materials in these devices must exhibit high electrical conductivity, rapid charge transfer, strong sensitivity, and stability.[52] In the case of self-powered wearable sensors, using nanomaterials or nanostructures can effectively improve the electrical performance of their electrodes.[53] In recent years, 2D materials have attracted considerable attention and have been extensively studied as promising candidates for biosensing and human health monitoring. Their exceptional physicochemical properties, such as high sensitivity, chemical stability, large active surface area, and biocompatibility, enable the development of biosensors with lower detection limits and enhanced performance.[54] Probably, one of the most studied materials in this field is graphene which is composed of atomic-sized single layers of covalently bonded carbon atoms and is mostly found in two forms: graphene oxide (GO) and reduced graphene oxide (rGO). GO is obtained *via* oxidation of graphene layers that introduce hydrophilic functional groups such as carboxyl, carbonyl, and hydroxyl, which provide higher reactivity, surface area, and functionalization capabilities. rGO is obtained *via* removing the oxygen from GO, resulting in a structure with high electrical and thermal conductivity, remarkable mechanical properties, and more chemical stability compared to graphene and GO.[55] The unique properties of graphene-based materials make them promising candidates in sensors and biosensors since different types of biorecognition elements could be attached to their surface. This surface functionalization enables enhanced sensitivity and specificity in detection and minimize background interference and noises that can enhance the performance of biosensors.[56,57] One possible drawback of graphene-based materials is that the sharp edges in their structure may impair their biocompatibility and increased cellular toxicity. However, these issues can be mitigated by different surface functionalization such as using hydrophilic polymers like polyethylene glycol.[58,59]

Transition metal dichalcogenides (TMDCs) are another group of 2D materials that are used in sensors. One of the most studied structures of this group is molybdenum disulfide (MoS_2), which has a layered structure composed of molybdenum and sulfur atoms. The structure of MoS_2 makes it a desirable material for biosensing due to its high surface area, functionalization capability, high sensitivity, and good biocompatibility.[60] MoS_2 nanosheets possess tunable optical and electrical properties that are dependent on the number of MoS_2 layers and the size of their band gap. Owing to the unique and controllable properties of MoS_2, there have been numerous studies focused on developing biosensors with high sensitivity that facilitate early diagnosis of biomolecules and cancer biomarkers.[61]

Layered double hydroxides (LDHs) are another class of 2D layered materials with a general formula of $[M_{1-x}^{2+}M_x^{3+}(OH)_2]^{x+}A_{x/n}^{n-}\cdot yH_2O$ in which M^{2+}, M^{3+}, and A^{n-} indicate divalent cations, trivalent cations, and *n*-valent anions, respectively.[62] The layered structure of LDHs is composed of octahedral crystal units containing hydroxide ions, M^{2+}, and M^{3+} ions, while the interlayer space is occupied with A^{n-} anions and water molecules. This structure has caused the LDHs to be vastly studied as potential biomaterials for sensing applications. The layered structure of LDHs offers high tunability with the ability to interlayer ion exchange and alter the interlayer space distance. In addition, it has been shown that various LDH structures demonstrate acceptable biocompatibility and low cellular toxicity. Moreover, the positively-charged LDH layers allow their surface modification and interaction with the negative charges on cell membranes or negatively-charged biomolecules. LDHs also have multiple advantages for biosensing because they show high sensitivity and low detection limit alongside good stability and reproducibility, while having a relatively low production cost.[63]

Lastly, MXenes, which are the main focus of this review, are a class of newly emerged 2D nanomaterials that have caught the attention of many researchers especially in the fields of biomedical engineering and biosensors due to their exceptional

properties such as high electrical conductivity, mechanical strength, chemical stability, and cellular biocompatibility and can be used in composite with different types of polymers, metals and their oxides, and carbon-based materials such as graphene.[64] The following subsections first discuss the chemistry and structure of MXenes and subsequently introduce different general wearable platforms and the factors affecting their comfort and performance, followed by the role of MXenes in enhancing the self-powering and detection of wearable devices.

3.2 Chemistry and structure of MXenes

MXenes are transition metal carbides, nitrides, or carbonitrides with the general formula $M_{n+1}X_nT_x$ (Fig. 5), where M is a transition metal (*e.g.*, Nb, V, or Ti), X is either carbon or nitrogen, T_x represents surface termination groups (such as –OH, =O, or –F), and n is the number of metal layers in the MXene structure, typically ranging from 1 to 4. The resulting layered structures possess high metallic conductivity from the transition metal carbide/nitride backbone, while the presence of surface terminations provides tunable hydrophilicity, surface charge, and chemical reactivity. The balance between a conductive core and a chemically functionalized surface gives MXenes a unique combination of electronic, mechanical, and interfacial properties that are advantageous for wearable energy devices.[65] MXenes are synthesized from a MAX precursor phase in which A is an element from the groups 12–16 of the periodic table, such as Al in Ti_3AlC_2 MAX precursor. In most studies, MXene is usually prepared by selectively etching a layer from the MAX phase using etchants like hydrofluoric acid (HF) to obtain multilayered MXene structures, followed by a delamination process (such as sonication) to obtain MXene nanosheets.[66] Delamination can also take place using eco-friendly solvents. For instance, Sankar *et al.* prepared MXenes using delamination in the eco-friendly Cyrene solvent with different sonication times (15, 30, 60, and 120 minutes), investigated the stability of the produced MXenes, and compared them with *N*-methyl-2-pyrrolidone (NMP) solvent. Their results indicated that 60 and 120 minute sonication times resulted in stable dispersions after 20 weeks of storage. Moreover, MXenes in Cyrene solvent showed less surface oxidation than in NMP during 6 month period. However, both MXenes, in Cyrene and NMP, showed toxicity on human skin cells that was mitigated after resuspending MXenes in BSA, showing that there are still concerns regarding MXene dispersion solvents.[67]

The chemical terminations in MXenes play a pivotal role in determining their electrochemical performance. For instance, oxygen-rich terminations enhance pseudocapacitive behavior through reversible redox reactions, while hydroxyl groups improve dispersion in aqueous media, facilitating the fabrication of flexible films and composites. Fluoride terminations, in contrast, may hinder ion transport and reduce capacity. Additionally, the layered structure of MXenes enables intercalation of ions and molecules, which is essential for energy storage devices such as supercapacitors and batteries integrated into self-powered wearables. The high electrical conductivity of MXenes, often exceeding 10 000 S cm^{-1}, ensures efficient charge transport, while their mechanical flexibility supports conformal integration into stretchable or bendable substrates.[68–70] Owing to the variety in surface functional

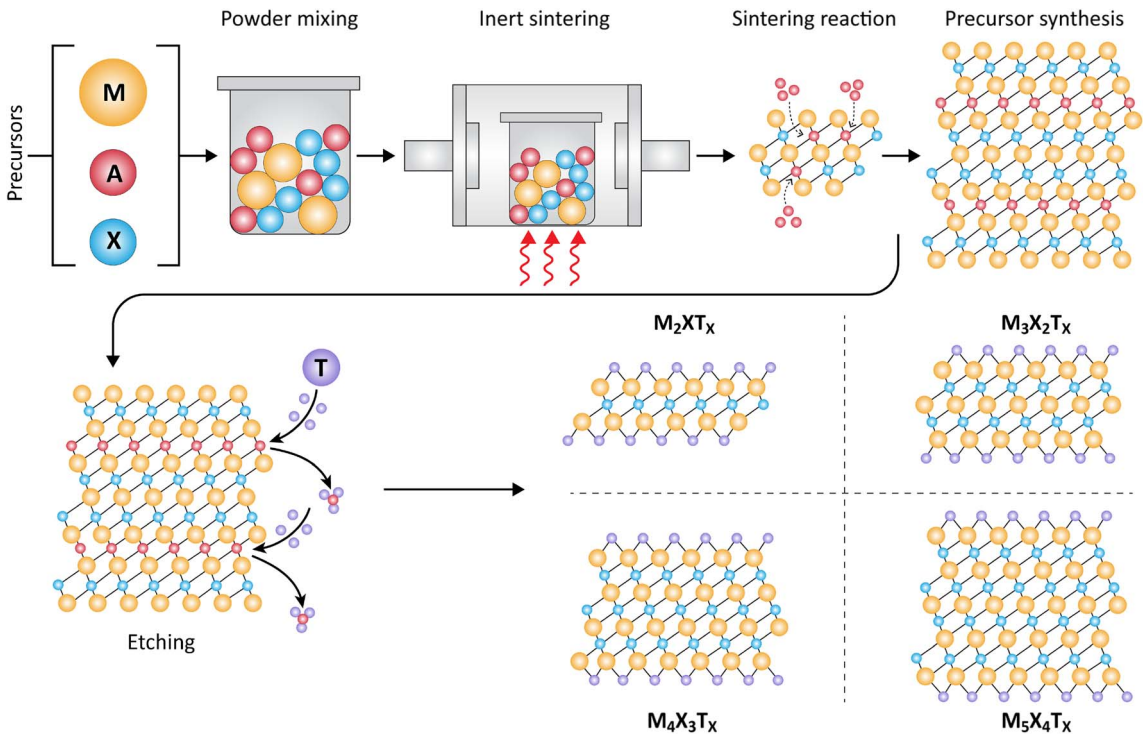

Fig. 5 Synthesis and chemical structure of MXenes.

groups, MXenes are capable of surface modification with different molecules to increase their functionality, especially with biomolecules such as proteins, enzymes, and DNA. These functionalization can either take place through covalent bindings (such as siloxane bonds from the reaction between the hydroxyl surface groups and silane-based molecules or amide bonds from the reaction between carboxyl moieties on the nanosheets surface and amine groups on different biomolecules like proteins through carbodiimide chemistry), or non-covalent interaction such as electrostatic interactions between a positively charged molecule and the negatively charged MXene surface.[71]

MXene layers are also susceptible to water attack and hydrolysis in aqueous media, as reported by Wu *et al.* in a study investigating the interaction of water molecules with oxygen-terminated MXene surfaces. They found that water adsorption on O-terminated planes promotes molecular dissociation, leading to the formation of Ti–OH bonds. This process displaces Ti atoms from their lattice positions, causing cleavage of Ti–C bonds and eventual structural hydrolysis. To mitigate this degradation, two strategies have been suggested: (1) introducing negatively charged moieties to repel water molecules, or (2) converting surface oxygen groups into hydroxyls to hinder water–MXene interactions.[72]

3.3 Design considerations for MXene-based wearable devices

3.3.1 General design factors for wearable devices. Several factors should be considered when designing a proper wearable device to obtain a functional product. One key aspect of wearable devices is their ease of use and comfort. A well-designed comfortable wearable device can also boost the device's performance and reduce signal noise and detection artifacts.[73] The mechanical properties of the desired substrate play a key role in its comfort. The substrate material should be flexible enough to be adapted to the skin and closely mimic the mechanical properties of natural skin. Indeed, inconsistencies between the skin and wearable device can lead to the loss of the interface between the device and skin, which subsequently decreases its accuracy. Furthermore, the substrate material should be tough and elastic with high stretchability to sense the applied strains.[74] Another key consideration regarding the substrate is its permeability. Generally, a wearable device should be impermeable to gas and liquid molecules that may degrade the device and hinder its performance while at the same time allowing for the exchange of oxygen and trapped water under the device to prevent its accumulation between the skin and device to increase its breathability.[75]

Proper adhesion to the skin is another feature that should be considered when developing a wearable device. Poor device adhesion to the skin can decline the performance of the device and cause signal artifacts. Therefore, it is essential to design and manipulate materials to achieve strong interfacial contact between the device and the skin. Adhesion can be achieved through chemical covalent bonds (*i.e.* imine, amide, or nitro bonds) or non-covalent hydrogen bonding, and electrostatic interactions.[76] Proper adhesion becomes a major challenge when skin is exposed to water since the boundary layer of water that forms on it prevents hydrogen bonding between the device and skin resulting in poor adhesion. For example, catechol groups in tannic acid were reported to facilitate the adhesion of a silk fibroin/polypyrrole (PPy) to various substances such as polytetrafluoroethylene (PTFE), glass, plastic, and pig skin by hydrogen bonding through the presence of phenol and hydroxyl groups, hydrophobic interactions, and electrostatic interactions.[77]

Various types of materials are used to create wearable sensors with high flexibility and adequate mechanical properties. Different kinds of synthetic polymers, such as polyethylene terephthalate (PET), PDMS, and polyimide (PI) are widely used as flexible substrates or as coating for wearable sensors because of their versatile fabrication methods, the ability to tune their mechanical properties, and their biocompatibility and safety for incorporation on skin. However, there are still limitations and concerns regarding their recyclability and sustainability.[78] Another major drawback of these polymers is their low thermal conductivity (0.2–0.4 W m^{-1} K^{-1}) which limits their use in self-powered wearables.[79] To overcome this obstacle, flexible polymer composites are made using thermal conductive fillers such as boron nitride (BN). Wang *et al.* created a flexible composite of PDMS with boron nitride fillers. It was demonstrated that increasing the amount of BNs in the composite by up to 30%, resulted in a gradual increase in the thermal conductivity of a TEG for a self-powered wearable pulse sensor due to the increased contact between BN particles and an increase thermal conductivity pathway.[80] Lin *et al.* prepared a 3D foamed network of PDMS and BN nanosheets by hot-pressing PDMS into a prepared PDMS/BN foam. They found that under a 25% volume fraction of BN in the foam, the thermal conductivity of this composite in the direction of BN nanosheets was 7.55 W m^{-1} K^{-1}, which was notably higher than randomly dispersed BN fillers (2.99 W m^{-1} K^{-1}) and pure PDMS (0.49 W m^{-1} K^{-1}).[81] Another concerning issue regarding these materials, especially those with an elastomeric nature, is that there is a mechanical mismatch between these materials and the natural skin as many studies reported that the elastic modulus of the natural skin lies in the order of kPa, while the elastic modulus of Sylgard is 184 PDMS, which is widely used in wearable devices, is in the order of MPa.[82–84] To address the downsides of these materials, hydrogels are also being investigated as promising substrates for wearable devices. Compared to other types of polymers and elastomers, hydrogels show more compatibility as they offer lower Young's modulus and high water content that can resemble the natural microstructure of the human body as well as being non-toxic towards the body.[85]

Using hydrogels as the substrate for wearables, it is possible to integrate substances that grant them electrical conductivity which is crucial in the development of self-powered wearable devices. This group of hydrogels, commonly known as conductive hydrogels, is prepared by either incorporating ionic salts (*i.e.* ionically conductive hydrogels) or conductive fillers (*i.e.* electrically conductive hydrogels).[86] Despite their advantages, hydrogels may lack sufficient mechanical properties for

wearable applications. The mechanical performance of hydrogels can be tuned in several ways to meet the needs of wearable devices. One such method is using hydrophilic fillers that can form hydrogen bonds with polymer chains in hydrogels. An example of such fillers is graphene oxide which is rich in oxygen-containing groups such as hydroxyl, carboxyl, carbonyl, and epoxy that can form hydrogen bonds with polymer chains and further improve their mechanical strength.[87] Fabricating dual-network (DN) hydrogels is another method to boost the mechanical performance of wearable hydrogels. These structures consist of a chemical network which is rigid and strong and a physically flexible network. Upon stretch, the physical network acts as a sacrificial bond that dissipates energy, and the chemical network helps retain the integrity of the structure.[88] Qu *et al.* prepared a DN wearable hydrogel based on *in situ* polymerization of acrylamide (AAm) and ionic bonds between Ca^{2+} ions and sodium alginate. They prepared different samples of hydrogels with polyacrylamide chains and free uncrosslinked sodium alginate chains (PAM/SA) and with ionically crosslinked sodium alginate chains (PAM/CA) in the water medium, and 30% ethanol medium (PAM/CA/$EtOH_{30}$). During stretching, uncrosslinked alginate chains in the PAM/SA sample showed slippage but ionically crosslinked chains of PAM/CA unzipped during stretch, causing energy dissipation. They found that the presence of ethanol in the system reduced the water content and swelling ratio of the hydrogels and more concentrated crosslinks which in turn increased their mechanical strength. The tensile strength PAM/CA/$EtOH_{30}$ was recorded at 581 kPa, which was 2.2 times higher than PAM/SA samples.[89]

Another group of synthetic polymers is conducting polymers (CPs) such as PPy, polyaniline (PANI), and PEDOT:PSS that show electrical conductivity owing to the presence of π-conjugated bonds in their chemical structure that facilitates electron transfer, leading to the formation of conductive pathways.[90–92] However, a major downside of CPs is their poor flexibility which limits their use in flexible wearable sensors. To effectively incorporate these materials in wearable sensors and benefit from their conductive nature while also achieving a flexible product, CPs are incorporated into flexible polymer matrices such as PDMS or hydrogels.[93]

To overcome the drawbacks posed by synthetic polymers, paper-based substrates are also being studied as another type of flexible material for wearable sensors. An advantage of paper substrates compared to synthetic polymers is their biodegradability and easy disposal. However, these materials may lack sufficient mechanical strength and electrical conductivity as a result, further modification and functionalization are required to obtain an operational wearable sensor.[94–96] For instance, a self-powering supercapacitor, driven by a microbial fuel cell was printed on Whatman filter paper by using a composite ink consisting of CNTs, nickel/tin nanoparticles (Ni/Sn NPs), reduced graphene oxide, and PEDOT:PSS hydrogel to improve the power generated by the fuel cells.[97]

3.3.2 The role and properties of MXenes in functionalizing wearable devices. In the context of self-powered wearable devices, the structural and chemical features of MXenes translate into multiple functional benefits. Their high conductivity and redox-active surfaces make them promising electrode materials for flexible supercapacitors and microbatteries, which can store and deliver power harvested from the body or environment. Furthermore, the presence of tunable surface groups enhances compatibility with polymers, hydrogels, and textiles, enabling the fabrication of stretchable energy storage units. The presence of hydrophilic groups such as –OH on the surface of MXenes enables these materials to form stable aqueous mixtures and inks while also being electrically conductive.[98–102] Furthermore, the electrical conductivity of MXene structures can be modified and modulated. For instance, the type of surface functional groups and abundance can be tuned to meet the needs of specific applications. Also, MXene structures can have a diverse range of electrical conductivity and metallic/semiconductor behaviors by varying the M atom in the precursor phase.[103] MXenes also serve as active components in TENGs and piezoelectric systems, where their surface chemistry modulates charge trapping and transfer, directly improving output performance. By combining high electrical performance with structural adaptability, MXenes act as multifunctional materials that bridge energy harvesting, storage, and sensing in next-generation wearable platforms.[104,105] MXenes can also be used in composite with other materials to improve the electrical performance of active layers. For instance, San Nah *et al.*, reported that the addition of MXene to a laser-burned graphene (LBG)/PDMS resulted in higher oxidation–reduction peaks measured with cyclic voltammetry (CV) and reduced charge transfer resistance (R_{ct}), from 2910 Ω for the bare LBG/PDMS to 1124 Ω after the incorporation of MXenes.[106] In another study, Salauddin *et al.*, showed that the initial surface potential of a wearable TENG device had a 17-fold increase when using MXene/silicone nanocomposites accompanied by additional MXene layers.[107]

The alignment of MXene can also be influential in the properties of the designed wearables. Feng *et al.* demonstrated that the anisotropic orientation of MXene sheets in PVA hydrogels can affect the mechanical and electrical properties of a pressure sensor (Fig. 6A). Freeze–thaw method was used to fabricate the gel form of the hydrogel. At the MXene concentration of 3 mg mL^{-1}, the tensile strength of the MXene/PVA hydrogel was 875 kPa in the direction parallel to MXene orientation, which was 2.2 times higher compared to the orthogonal direction. In a similar manner, the compression strength in the parallel direction was 1.36 times higher than in the orthogonal direction (Fig. 6B). Furthermore, the ordered structure of MXene sheets resulted in a short distance between MXene nanosheets and an increase in the conductivity in the parallel direction, about 56 mS m^{-1} which is also 1.3 times higher than the perpendicular direction. Moreover, the MXene content also had a notable impact on the mechanical properties of the prepared hydrogels. Several concentrations of MXenes, ranging from 0.5 to 4 mg mL^{-1} in the parallel direction of the hydrogels were investigated and it was found that the G' and G'' of the hydrogels were increased gradually with increasing the content of MXene. On the other hand, changing the amounts of PVA could affect the strength of hydrogel so that the amounts of G' and G'' were increased by increasing the amounts of PVA. A

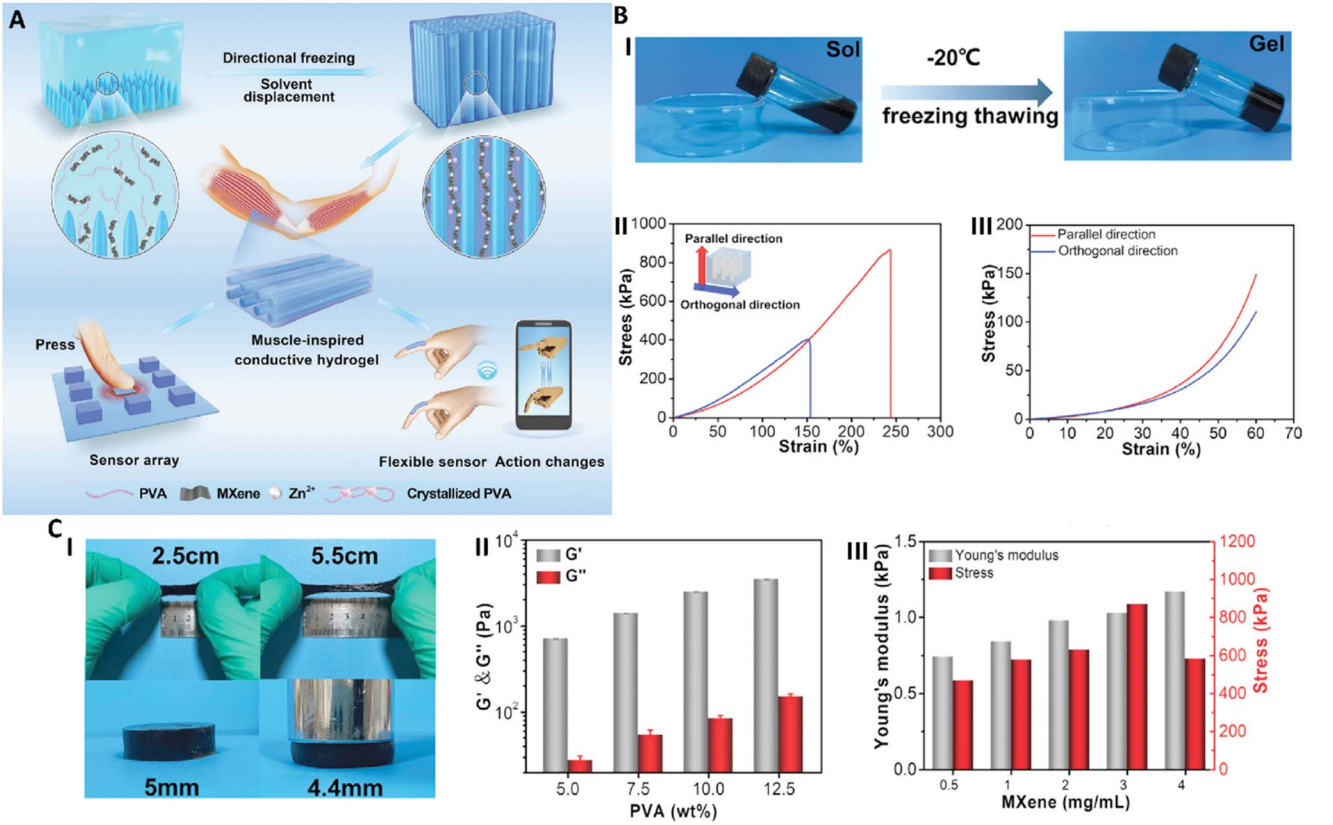

Fig. 6 (A) Schematic of the MXene-embedded PVA hydrogel with anisotropic MXene alignment; (B) transition of the MXene/PVA solution to gel by freeze–thawing at −20 °C (I) and the mechanical response of the composite hydrogel in parallel and orthogonal directions when subjected to tensile (II) and compressive (III) stress, at MXene concentration of 3 mg mL^{-1}; (C(I)) demonstration of the stretchability and compressibility of the composite hydrogel and the effect of MXene concentration on the storage and loss moduli, (II) Young's modulus, and fracture stress (III) in the parallel direction. Reprinted with permission from ref. 108. Copyright 2021, Wiley.

similar trend was seen in the values of Young's modulus and fracture stress of hydrogel. However, while Young's modulus kept increasing with the amount of MXene in the system, the fracture stress dropped when the MXene content was 4 mg mL^{-1} which was mainly due to the aggregation of MXene nanosheets in higher concentrations (Fig. 6C).[108]

Mao *et al.* reported a self-powered TENG electrode by incorporating Ti_3C_2 MXenes in a gelatin matrix. In this patch, the gelatin hydrogel was prepared using a transglutaminase crosslinker which provided adequate flexibility and MXenes enhanced the electrical conductivity of the electrode. They found that the concentration of MXene was a factor influencing the electrical properties of the electrode. The increase in MXene concentration from 5 wt% to 10 wt% showed an improvement in the open-circuit voltage (V_{oc}) and raised it from 152.8 V to 163.7 V. This trend was similar for the short-circuit current (I_{sc}) and was increased from 6.5 μA to 8.1 μA. However, further addition of MXene to a concentration of 15 wt% led to a drop in both V_{oc} to 143.8 V and I_{sc} to 7.4 μA. It was suggested that this decrease was the result of MXenes aggregation which limited charge transfer in the system.[109] A similar observation was reported by Yang *et al.*, in a self-powered stretchable TENG, in which PDMS–Ecoflex substrates were incorporated with MXenes to create the negative triboelectric layer of the powering unit when it encountered nylon fabric as the positive layer. It was found that the incorporation of MXenes had a notable impact on enhancing the electrical performance of the TENG. In MXene concentrations varying from 1–5 mg mL^{-1}, the V_{oc}, I_{sc}, and charge transfer density were increased from 20 V to 40 V, 5.3 mA m^{-2} to 10.6 mA m^{-2}, and 34.8 μC m^{-2} to 69.1 μC m^{-2}, respectively, when a force of 15 N was applied at 5 Hz frequency. However, they witnessed a minor drop in the trend of improvements when MXene concentration was raised beyond 5 mg mL^{-1} which again rose from the aggregation of MXene nanosheets.[110]

There are several methods to integrate MXenes with flexible substrates. Dense MXene layers can be added to porous flexible substrates through simple vacuum filtration of MXene mixtures on the substrate.[111,112] Yang *et al.* developed a flexible hybrid film consisting of Nb_2CT_x MXene, carbon nanotubes (CNT), and PEDOT on a PTFE substrate using vacuum filtration to develop a TENG system. The working mechanism of TENG in this sensor was based on vertical contact separation in which the hybrid film and PTFE substrate formed the lower and upper layers, respectively. Upon contact, a positive charge was induced in the hybrid film while the PTFE layer gained a negative charge. After separation, the electric field between these two layers altered due to the change in the distance between these two layers

therefore generating current from the hybrid film on the upper layer to the hybrid film on the lower layer to balance the positive charges. The next contact between the layers causes the electrons to move from the lower layer to the upper one, creating an opposite current. The weight ratios of Nb_2CT_x to PEDOT were investigated and it was found that equal ratios of Nb_2CT_x to PEDOT (1 : 1) can provide the best electrical properties for this hybrid film, with an open-circuit voltage of 125.8 V and a short-circuit current of 325 nA. Moreover, it was demonstrated that adding 1 milligram of CNTs had a synergic effect on improving the electrical properties of the film, raising V_{oc} to 184.1 V and I_{sc} to 4.42 μA.[113]

Negative charges on the surface of MXenes enable their electrophoretic deposition (EPD) on substrates. This was shown by Zhang *et al.*, where a composite mixture of $Ti_3C_2T_x$ and EDOT was successfully deposited on LIG electrodes since the negative groups of MXenes allow them to be deposited on the substrate on the positive electrode. Compared to methods such as drop-casting, which showed a nonuniform deposition and aggregation of MXenes, the sensor prepared by EPD had a smoother and more uniform surface pattern which shows that EPD is a more advantageous method compared to some conventional deposition methods (Fig. 7A). The fabricated sensor was used in areas of the body that have no such movements to provide more accurate and reliable results. The fabricated formulation (LIG/MXene-$Ti_3C_2T_x$@EDOT composite) showed a clear and stable decrease in resistance with rising temperature, demonstrating a high temperature coefficient of resistance (TCR) of 0.52% K^{-1}, better than many existing thermistors. Its design reduced the effects of thermal expansion, maintaining stable performance even during repeated heating and cooling cycles, which confirmed its reliability and accuracy as a stretchable, strain-insensitive temperature sensor. It was also tested for the electrocardiogram (ECG) signal monitoring and showed excellent performance due to its high conductivity and low skin-contact impedance (51.08 kΩ at 10 Hz), that were much lower than traditional Ag/AgCl electrodes. Indeed, it showed the strongest ECG signal, with the highest QRS complex value of 0.74 mV, providing superior results to both the pristine LIG dry electrode and the Ag/AgCl gel electrode (Fig. 7B).[114]

3D printing using direct writing (DIW) of MXene inks is an effective method to create MXene complex and tailor-made MXene patterns on various substances with high precision.[115] From a rheological perspective, the hydrophilic nature of MXene surface functional groups allows them to form stable colloids in aqueous medium and gel-like inks at high concentrations which can be utilized in 3D printing fabrication methods.[116] In 3D printing fabrication of MXene electrodes, the rheological properties of MXenes inks, especially elastic modulus (G'), which indicates the elastic behavior of the ink, and loss modulus, which indicates the viscous behavior (G''), are studied to investigate how the designed ink flows under high shear rates during the printing process and its ability to retain its shape after the printing procedure is complete.[117] To obtain an optimal 3D printable ink, the rheological properties of MXenes may need to be tuned using different additives such as polymers[118] or divalent ions such as Zn^{2+} (ref. 119) for specific applications.

Electrospinning is a common technique to produce versatile micro/nanofibrous polymeric structures with tunable mechanical properties and architectures (including pore size and geometry). Electrospinning polymeric materials with MXenes as dopants is another approach to introduce MXenes to various substrates to fabricate self-powered wearables.[120] Zhang *et al.* prepared self-powered piezoelectric pressure sensor nanostructures by electrospinning PVDF containing MXene and ZnO nanoparticles. Different structures of PVDF/MXene and PVDF/ZnO were prepared such as double-layer, interpenetrating, and core–shell structures. The electrospun fiber mats were assembled on a nylon-11 fiber membrane and a polyurethane (PU) film, accompanied by conductive tapes to fabricate the flexible structure. A positive effect on the piezoelectric properties of the electrospun structures was seen when increasing the MXene concentration up to 3 wt%. The output voltage of PVDF/MXene composite with 3 wt% MXene content was 3.52 V at a frequency of 2.5 Hz and under a force of 11.0 N. It was also demonstrated that the core–shell structure with 2 wt% ZnO as the core and 3 wt% MXene as the shell showed the highest output voltage of 4.8 V. The primary reason behind this optimal result is that the MXenes in the shell could rapidly transfer the produced charges from the fiber mat to the electrode due to their high electrical conductivity.[121]

Similarly, Huang *et al.*, prepared PVDF/MXene dispersions in dimethylformamide (DMF)/acetone solvent and prepared a composite mat which was used in TENG wearables as the negatively charged triboelectric layer. It was found that the addition of MXenes to PVDF could efficiently increase the V_{oc} and I_{sc} of the negative triboelectric layer since MXene created a highly negative surface due to the presence of –F and =O electronegative surface groups. In addition, the optimal MXene content was found to be 6 wt%, after which no notable improvement was detected due to the possible saturation of MXene beyond that concentration.[122] Bhatta *et al.* investigated how the presence of MXenes in electrospun PVDF-based TENG can affect its dielectric constant. They measured the dielectric constant for pure PVDF and PVDF with 5, 10, 15, 20, and 25 wt% of MXene blends at a frequency of 1 kHz. With the addition of MXenes, the dielectric constant of the fibers increased from 13.35 for pure PVDF to 45.78 for PVDF with 20 wt% of MXene, with a minor drop to 44.10 when the MXene content was further increased to 25 wt%. The primary cause for this increase was due to the polarization of MXene surface atoms with hydrogen atoms in PVDF chains within an external electric field.[123]

The incorporation of MXenes with hydrogels is a promising approach to fabricating functional wearables. By incorporating MXenes with hydrogels, it is possible to obtain structures with high electrical conductivity, surface area, and tunability while being mechanically stretchable and flexible, with high water content and microstructure that closely resembles the human body.[124] As a result, MXene–hydrogel composites are auspicious candidates to fabricate self-powered wearable devices. A flexible conductive hydrogel-based TENG electrode was fabricated by Long *et al.*, by the polymerization of acrylamide (AAm)

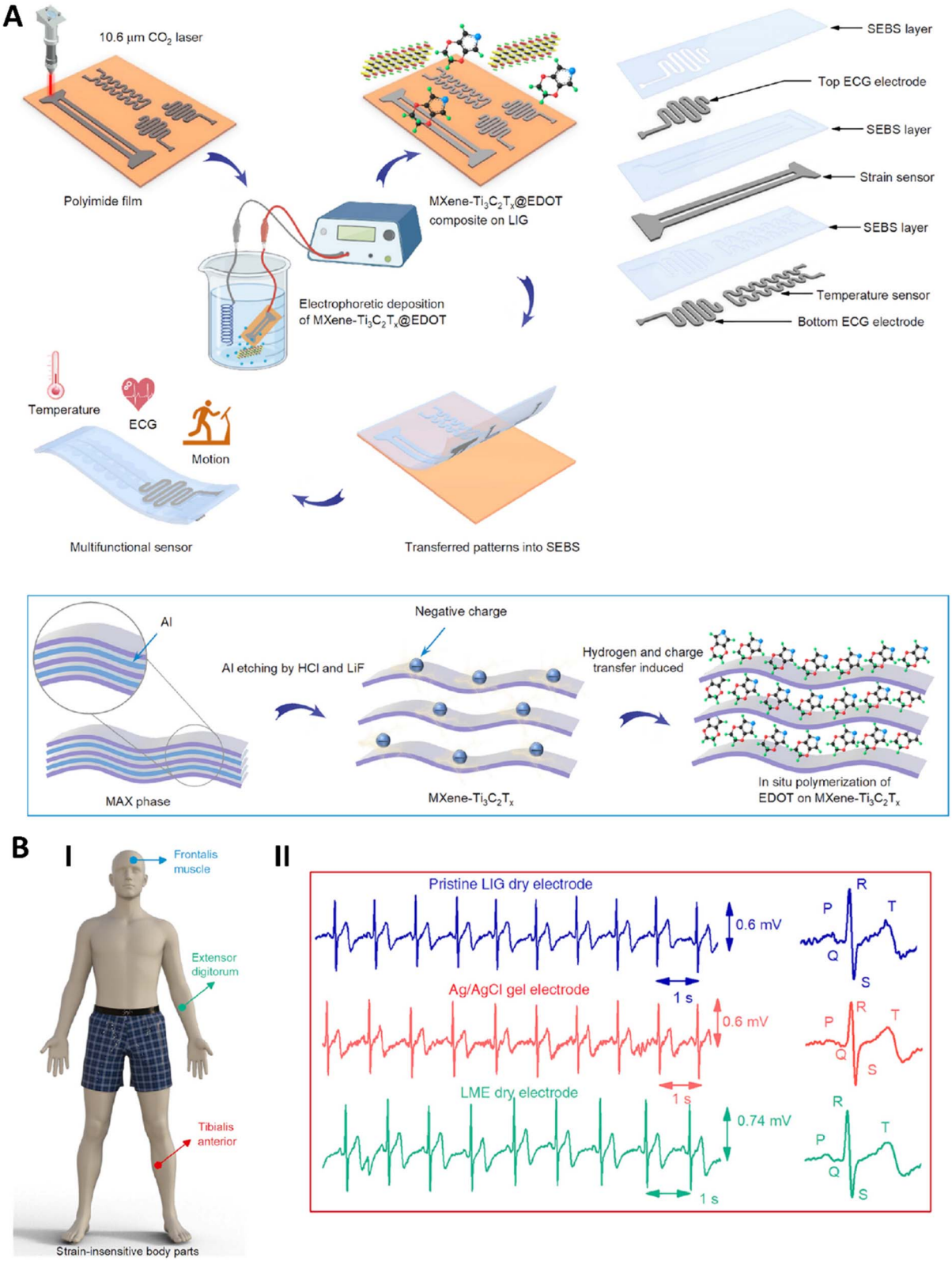

Fig. 7 (A) Schematic image related to the fabrication of LIG/MXene-$Ti_3C_2T_x$@EDOT sensor. (B) Schematic image related to measurement of temperature from strain-insensitive of body parts (I). Utilizing different electrodes (including Ag/AgCl gel, LIG, and LIG/MXene-$Ti_3C_2T_x$@EDOT electrodes) for checking ECG (II). Reprinted with permission from ref. 114. Copyright 2022, Nature.

monomers using ammonium persulphate (APS) and *N*,*N*′-methylene bisacrylamide (BIS) crosslinking agent in a PVA solution and adding MXene suspension to the hydrogel matrix. They found that in addition to the chemical crosslinking between AAm monomers and physical crosslinking with PVA chains, MXenes nanosheets also provided additional crosslinks because of hydrogen bonds between their MXenes surface functional groups and PVA and PAAm chains. To evaluate the TENG performance of this hydrogel composite, they measured the values of I_{sc}, V_{oc}, and the transferred charge (Q_{oc}) of the electrification process. It was found that I_{sc}, V_{oc}, and Q_{oc} were 2 μA, 40 V, and 15 nC, respectively for hydrogel without any MXene content, and these values reached the peak when 0.4 mL MXene suspension was added to the hydrogel precursor solution, reaching 10 μA, 180 V, and 65 nC, respectively. However, this increase in TENG output performance was not consistent and the performance of the hydrogel electrodes declined when MXene content increased beyond 0.4 mL up to 1 mL.[125]

Spray coating MXene mixtures is another method to introduce MXene to flexible substrates. Ding *et al.* prepared an electrospun PVDF/CNC substrate and used spray coating to deposit MXene on its surface. They showed that the number of spraying cycles can affect the electrical conductivity of the substrate. Several numbers of sprays namely 5, 10, 15, 20, 25, and 30 times were investigated and it was found that as the number of sprays increased, the electrical conductivity of the substrate also increased; however, the significant boost in electrical conductivity was observed within 5 to 20 times of spray and beyond that, the increase in electrical conductivity was marginal.[126]

3.4 Challenges in device fabrication and scalability

Despite the promising properties of MXenes in fabricating wearable devices, there are still several issues that need to be addressed. Probably, one of the most notable gaps between laboratory and industry is the scalability of MXenes as they are produced in small batches for research purposes.[127] Small-scale MXene fabrication cannot meet the needs to achieve industrial fabrication of MXene-based wearables, and fabrication methods with high-throughput production of MXenes are required to meet this goal. To prepare MXene films in a scalable manner, Salles *et al.*, used a continuous blade coating system to deposit a mixture of MXene and silk sericin on a PET substrate.[128] MXenes are also susceptible to oxidation and hydrolysis in humid conditions and the presence of oxygen and formation of metal oxides such as TiO_2 which can have adverse effects on the properties and performance of devices. For instance, the formation of TiO_2 and reducing the connectivity between the lamellar structures of MXenes can decrease their electrical conductivity. Moreover, the presence of TiO_2 and titanium vacancy defects can also negatively impact the mechanical properties of MXene sheets by diminishing their flexibility and strength.[129,130] Therefore, to be able to produce MXene-based wearables on an industrial scale, the long-term stability of MXenes still needs to be addressed and studied. To prepare MXenes with higher structural and chemical stability, Zhang *et al.*, modified MXene flakes with PEI/$AgNO_3$ crosslinks to fabricate a humidity sensor. It was found that this modification resulted in better stability of the sensor during 30 days under different humidity conditions. It was found that only 5.57% of the sensor capacitance response was lost after this period and under a relative humidity of 97% which indicated high chemical stability of this sensor, mostly due to the presence of oxygen moieties in the PEI/$AgNO_3$ that prevented oxidation reactions.[131]

Safety is also a major concern when it comes to producing MXene on large industrial scales. One of the key concerns is the use of hydrofluoric acid (HF) during the synthesis process of MXenes. There are several risks associated with HF. HF is a strong acid and can cause severe burns and damage to body tissues upon exposure even at low concentrations. As a result, it is crucial to have necessary safety equipment such as personal protective equipment (PPE) like gloves, protective glasses, and shields. Handling post-synthesis waste is also an important safety and environmental challenge as it must be handled and disposed of in compatible containers.[132] While these issues can be tackled in small-scale laboratory conditions, they might be challenging to resolve when it comes to mass production of MXene-based wearables on an industrial scale since more controlled guidelines are required to ensure the safety of staff and minimize the harmful impact of HF waste on the environment. Interestingly, instead of discarding the waste material during the MXene synthesis process (*i.e.* unetched MAX phase or unexfoliated MXenes after delamination), Ma *et al.* used these waste products (referred to as "trash") to fabricate a pressure sensor. The waste sediments after MXene synthesis were collected and screen-printed on a cellulose substrate. These waste products were able to operate under low voltages of 0.05 V with a sensitivity of 0.56 kPa^{-1}.[133]

Aside from the complications regarding MXenes, wearable systems also face several challenges for industrial production. These challenges include the possible toxicity of materials used as energy generators and their biocompatibility.[134] Moreover, the power generated by most self-powering sources is still inferior compared to batteries. This issue may impair long-term commercial applications of these devices and requires further research to develop sustainable self-powering sources to be able to commercialize self-powered wearable devices.[135]

Hydrogel-based wearables also suffer from low performance and sensitivity under severe environments, and their application is limited especially in freezing temperatures due to their high-water content. A possible solution to this issue was studied by Liu *et al.* who developed a hydrogel-based wearable with TENG and PENG energy harvesting mechanisms using PVA as the hydrogel matrix and MXene/cellulose nanofibers (CNF) as conductive microchannels embedded within the hydrogel. To boost the performance of their sensors under harsh conditions (like high and low temperatures), they added glycerol, an anti-freezing and moisturizing agent to the hydrogel composite. They found that the hydrogels containing glycerol could maintain their initial flexibility and elasticity at a temperature of −20 °C while the samples without glycerol froze and became brittle. Additionally, at the temperature of 60 °C, the hydrogels

containing glycerol almost retained their initial volume and only lost 16.7% of their water content after 5 days.[136]

4 Biomedical applications of MXene-based self-powered wearable devices

The high conductivity, mechanical robustness, and surface chemical groups of MXene have shown great promise in the design of next-generation sensors. Surface modification, such as functionalization by groups like hydroxyl or carboxyl is an important factor for biosensing applications that enhance dispersibility in aqueous environments.[19]

4.1 Physiological monitoring and health tracking

He *et al.*,[137] designed a self-healing and highly sensitive polysaccharide/$Ti_3C_2T_x$ MXene nanosheet into chondroitin sulfate (CS)/*N*,*N*-dimethylamino ethyl acrylate (DMAEA-Q) hydrogel for multifunctional sensor applications. This hydrogel exhibited excellent stretchability, rapid self-healing within 60 s, enduring strains of over 5000%, and perfect adhesion with an adhesive strength of approximately 100 kPa. The electrical conductivity was 5.33 S m^{-1}, which allowed real-time monitoring of mechanical signals with a strain range of 50–400%. This hydrogel showed a rapid photothermal response, with temperature exceeding 55 °C under light exposure, and can work as a humidity sensor, detecting human respiration *via* resistance changes in response to humidity variations (10–80% relative humidity).

A 3D-printed self-powered MXene-based physiological sensing system was designed in another research that included triboelectric nanogenerators (M-TENGs) for power generation, capacitive pressure sensors (M-PS) for physiological signal monitoring, and wireless data transmission using near-field communication (NFC). MXene ($Ti_3C_2T_x$) paired with a skin-like styrene–ethylene–butylene–styrene (SEBS) showed an excellent triboelectric property and high stretchability. Peak power density, open-circuit voltage, and short-circuit current were 816.6 mW m^{-2} at an optimal load of 10^8 Ω, 8 Hz, and 19.9 N. The M-TENG successfully powered 80 LEDs in a series using energy harvesting from biomechanical movements. This device can detect real-time radial artery pulse waveforms successfully. The high sensitivity, rapid response time, and wireless data transmission capabilities of the fabricated sensor made it a promising candidate for wearable healthcare applications.[138]

In another study, Lee *et al.*,[139] developed a lightweight, fabric-based lamina emergent MXene-based electrode (FLEXER) for wearable electrophysiological monitoring (Fig. 8A). The FLEXER design adhered to skin stably through a shape-morphing mechanism that self-assembled with pneumatic pressure. The FLEXER exhibited excellent electrochemical performance, exceptional durability over 1000 bending cycles, outstanding mechanical stability, and strain resistance up to 15%. This electrode, made of MXene combined with cellulose nanofiber (CNF) and polycarboxylate ether (PCE) (MXene/CNF/PCE), demonstrated a low resistance of 24.7 Ω m^{-1} and maintained electrical stability under 15% strain, with a minimal resistance increase (R/R_0 = 2.1). It recognized hand gestures with a 95.94% accuracy using electromyography (EMG) and a convolutional neural network. The monitoring system developed with FLEXER showed ECG signals comparable to traditional electrodes, achieving a signal-to-noise ratio (SNR) of over 20 dB. The skin-electrode impedance at 100 Hz was 191 kΩ, which was close to dry Ag/AgCl electrodes (190 kΩ), and oxidation stability was 20× better than normal MXene (Fig. 8B). This composite enhances durability in humid environments, with R/R_0 increasing only to 65 after 17 days in 100% humidity. These results maintained FLEXER's potential for reliable, noninvasive, and can be used in health monitoring, prosthesis control, rehabilitation, and smart wearables, integrating seamlessly into daily life. The FLEXER device was connected to a flexible circuit board to collect, amplify, and wirelessly transmit ECG signals in real time *via* Bluetooth. Despite being worn over clothing, the FLEXER achieved strong skin contact and high signal quality due to its pneumatic structure, producing ECG waveforms similar to those from commercial Ag/AgCl electrodes. It also effectively tracked heart rate changes before and after exercise and provided more comfort for long-term use since it only contacts the skin during measurements. It also provided stable real-time ECG signals during various activities like standing, walking, and driving once activated (Fig. 8C–E).

4.2 Sweat analysis and biochemical sensing

Conventional techniques such as chromatography, immunoassays, and mass spectrometry, which are widely used for biomarker detection, toxicity assessment, and therapeutic agent tracking, face several limitations. Limited shelf life, long assay durations, suboptimal reproducibility, signal instability, and high sample size are some existing challenges. However, electrochemical sensors offer distinct advantages, including small-scale fabrication, operational simplicity, high sensitivity, and cost-effectiveness, making them highly suitable for continuous and real-time biomarker monitoring.[140] Electrochemical biosensors employed biological recognition elements to achieve highly sensitive and selective detection of target analytes with low detection limits. These biosensors operate on the principle that the interaction between immobilized biomolecules and the target analytes induces alterations in the electrical properties of the sensing material or solution. These changes, which may include variations in conductance, potential, electrical, or ionic strength, can be measured using techniques such as amperometry, potentiometry, voltammetry, and impedance analysis. MXenes with high electrical conductivity, excellent ion transfer, and biocompatibility are recognized as advanced biosensing tools that can detect ions, small and large biomolecules, and even cells. Generally, enzymes are immobilized on the MXene nanosheets to catalyze the chemical reaction of the molecules.[141] Wearable electrochemical biosensors are promising noninvasive monitoring that can measure sweat metabolites such as alcohol, glucose, lactate, sodium, and potassium ions.[142]

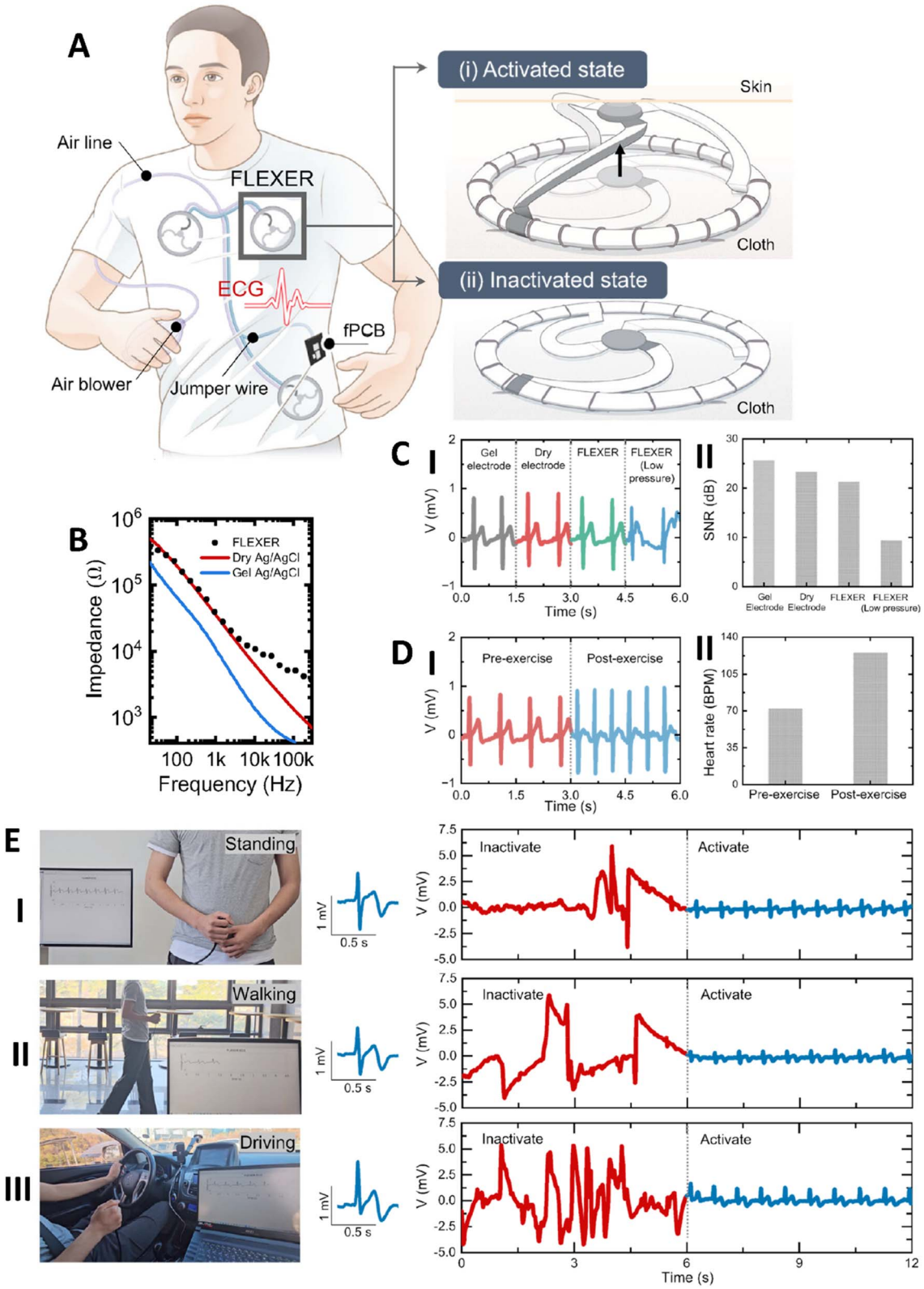

Fig. 8 (A) Schematic image of controllable FLEXERs used for ECG monitoring in activated and inactivated states. (B) Skin impedance comparison between pneumatically fully activated FLEXER and the dry and wet Ag/AgCl electrodes. (C) Comparing the record of different electrodes detected by (I) ECG signals (II) and SNR values. (D) Results of (I) ECG signals and (II) heart rate of FLEXER electrode recorded before and after exercise. (E) Results of ECG real-time using active and inactive multi-FLEXER in different situations, including (I) standing, (II) walking, and (III) driving. Reprinted from ref. 139 under the terms of the Creative Commons CC BY license. Copyright 2024, The Author(s).

Vaghasiya *et al.*,[143] developed a wearable flexible supercapacitor (FSC) patch that leveraged MXene Ti_3C_2 nanosheets and a polypyrrole–carboxymethylcellulose (Ti_3C_2@PPy–CMC). The fabricated composite was an active electrode material that utilized sweat as a biocompatible electrolyte, addressing the toxicity concerns of traditional electrolytes in wearable devices. Treating the patch's surface with –F and –OH functional groups led to uniform coating of composite on the surface of PCBC. The specific capacitance (C_{sp}) achieved by the Ti_3C_2@PPy–CMC composite reached up to 160 F g^{-1}, surpassing the values of pristine Ti_3C_2 (134 F g^{-1}) and PPy–CMC (94.4 F g^{-1}). Furthermore, the device displayed an energy density of 2.23 Wh kg^{-1} at a power density of 99.9 W kg^{-1}, which reduced to 1.17 Wh kg^{-1} as the power density increased to 498 W kg^{-1}. These metrics highlighted significant improvements compared to previously reported sweat-electrolyte-based supercapacitors. The device maintained excellent mechanical flexibility, retaining 99% of its original capacitance after 2000 bending cycles. Practical tests confirmed its capacity to power small electronic devices, such as LEDs and glucose meters, utilizing sweat from various body regions.[143]

A non-invasive electrochemical copper(II)–tetra(4-carboxyphenyl)porphyrin iron(III)/MXene (Cu–TCPP(Fe)/MXene) sensor (or MMs Paper-ECL sensor) was developed for glucose and uric acid detection. The sensor surface was modified with glucose oxidase (GOD) and uricase (UO) enzymes, which catalyzed the oxidation of glucose and uric acid. These reactions produced hydrogen peroxide (H_2O_2), which was essential for electrochemical detection. It provided high accuracy with recovery rates of 95.10–102.54% for glucose and 94.80–102.39% for uric acid, with relative standard deviations (RSD) below 10% across artificial sweat, urine, and saliva samples, which made it stable for up to 100 days. The interfacial interactions significantly enhanced the stability and catalytic performance of the sensor. Compared with traditional sensors, the MMs Paper-ECL sensor offered high accuracy, linear detection ranges from 0.001 nM to 5 mM, 0.025 nM–5 mM, and wonderful stability for up to 100 days with detection limits as low as 1.88 am and 5.80 pm. The charge transfer resistance (R_{ct}) was reduced to 1995 Ω, compared to 6517 Ω for unmodified electrodes. Therefore, this electrochemical sensor showed the potential for real-time diagnostics of metabolic disorders, such as diabetes and hyperuricemia, with broad applications in wearable health monitoring.[144]

MXene/Prussian Blue ($Ti_3C_2T_x$/PB) composite was used to produce a real-time wearable biosensor for the detection of glucose, lactate, and pH levels in human sweat with high sensitivity and accuracy. This sensor incorporated a solid–liquid–air interface, ensuring a constant oxygen supply to enhance enzyme activity and solve traditional sensor oxygen challenges. The detection areas of glucose and lactate were reported as 35.3 μA mm^{-1} cm^{-2} and 11.4 μA mm^{-1} cm^{-2}, and the detection limit were 0.33 μM and 0.67 μM, respectively. The hydrogen peroxide sensitivity was 52.3 μA mm^{-1} compared to CNTs/PB (40.5 μA mm^{-1}) and graphene/PB (29.7 μA mm^{-1}). The pH sensor indicated a sensitivity of −70 mV per pH with good linearity (R_2 = 0.998). During on-skin testing, the biosensor demonstrated efficient performance, which can collect and detect sweat (sensor activation) in less than 2 minutes. Also, the sensor monitored physiological changes between 10 to 30 minutes during the cycling test.[142]

Another biomarker detection was a wearable electrochemical immuno-sensor with a microfluidic system based on $Ti_3C_2T_x$ MXene-loaded laser-burned graphene (LBG) flakes for noninvasive cortisol biomarker detection in human sweat. The substrate was fabricated by polydimethylsiloxane (PDMS) for skin attachment, and electrodes were manufactured using LBG and modified by $Ti_3C_2T_x$ MXene and specific antibody (Fig. 9A and B). Cortisol antibodies were attached to MXene for sweat detection. Different electrochemical methods were used to detect the performance of fabricated electrode in detection of cortisol (Fig. 9C). The detection range and detection limit of cortisol sensing were 0.01 to 100 nM and 3.88 pM, respectively. The sensor exhibited an R_{ct} of 1124 Ω after $Ti_3C_2T_x$ MXene incorporation which was increased to 1750 Ω after antibody immobilization. $Ti_3C_2T_x$ MXene/LBG cortisol sensor had RSD percentage of 4.6%, which showed its acceptable reproducibility for cortisol detection. In sweat sample testing, recovery rate ranged from 93.68% to 99.1%, made it proper for point-of-care cortisol biomarker detection. The sensor demonstrated high selectivity, with negligible interference from other hormones like aldosterone, corticosterone, and progesterone.[145]

4.3 Disease detection and diagnostic capabilities

With a growing interest in personal wearable health monitoring, there is an increasing demand for real-time physiological condition tracking. MXene-based wearable devices have improved sensor sensitivity and selectivity, which can be seamlessly integrated into the body, enhancing interaction with skin, decision-making, and sensory perception. These characteristics have expanded their applications in human physiological activity detection, health monitoring, disease diagnosis, and clinical treatment. One of the applications of MXene wearable devices is glucose monitoring, which plays a critical role in the prevention and treatment of diabetes. The development of accurate and efficient glucose sensors is essential for precisely tracking glucose levels.[146,147]

MXene functionalized with TiO_2-integrated polymer dots (PD-MX/TiO_2) was used to generate a reactive-oxygen-species-responsive (ROS-responsive) hydrogel that could produce heat and control conductivity for cancer detection. The fabricated sensor showed H_2O_2 and photocatalytic responsive capabilities resulted from the presence of MXene and TiO_2, respectively. In other words, in the presence of H_2O_2 and visible light irradiation led to reducing size, an enhancement in swelling ratio, improving oxidation, reducing the toughness, and increasing the elasticity of PD-MX/TiO_2 hydrogel. Results of photothermal effect showed increasing in temperature by increasing the power of NIR laser irradiation and the number of MXene layers and decreasing by the addition of H_2O_2. The hydrogel's resistivity increased from 27.5 kΩ to 72.0 kΩ and 48.1 kΩ after exposure with H_2O_2 and visible light, respectively. It also showed LOD of about 28.63 μM for H_2O_2 detection, high

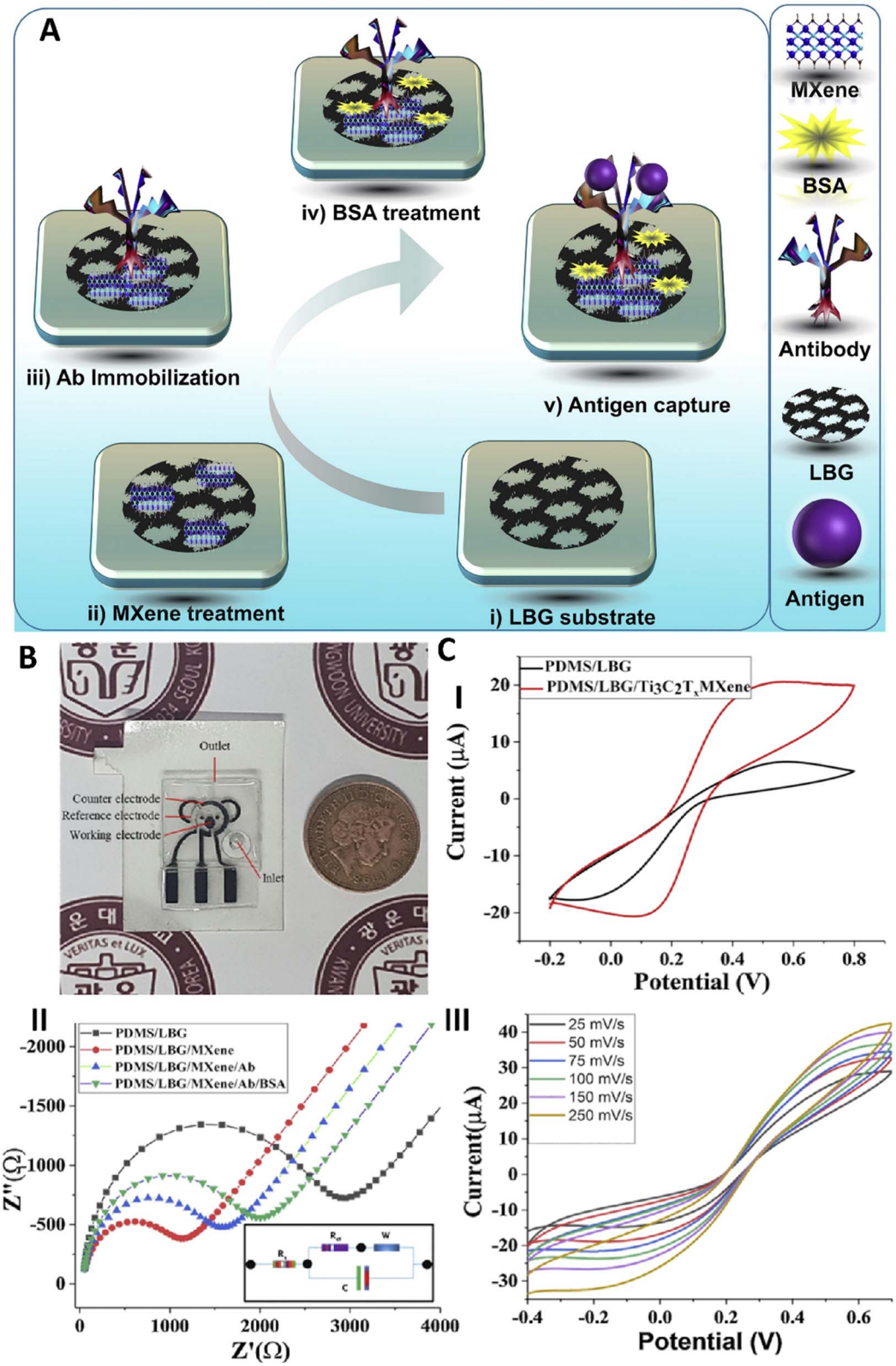

Fig. 9 (A) Schematic image of fabrication of $Ti_3C_2T_x$ MXene-loaded/LBG-based cortisol sensor; (I) laser-burned graphene (LBG); the LBG substrate (I) was functionalized with MXenes (II) followed by immobilization of antibody (AB) (III), addition of bovine serum albumin (BSA) (as the blocking compound) (IV). In the presence of cortisol, as the antigen, it could be captured by the AB immobilized on the surface of the sensor and provide a signal for detection (V). (B) An image of the wearable device. (C) Analysis of the sensor using (I) cyclic voltammetry (II) electrochemical impedance spectra, and (III) diffusion-controlled assay. Reprinted with permission from ref. 145. Copyright 2020, Elsevier B.V.

stability, and RSD percentage of 4.47% for 1 mM H_2O_2. Due to its sensitivity to H_2O_2, the fabricated hydrogel was then used to detect microenvironment of cancer *via* assessment of changes in pressure sensitivity, photothermal conversion, and conductivity. In comparison to normal cell lines, exposing cancer cells led to the enhancement of resistance of hydrogel resulted from the presence of higher amounts of H_2O_2 in the environment of cancer cells compared with normal cells that degraded the MXene *via* oxidizing them. The findings of this study suggested that the fabricated hydrogel hold great potential for real-time, direct cancer diagnosis when integrated with a wireless device connected to a smartphone, paving the way for advanced cancer detection.[148]

Hroncekova *et al.*,[149] constructed a $Ti_3C_2T_x$ MXene/chitosan nanocomposite biosensor for sarcosine detection, a potential prostate cancer biomarker in artificial urine. The biosensor showed a low detection limit of 18 nM, with a linear range up to 7.8 μM and a response time of 2 s. During sarcosine detection in artificial urine, the recovery index of biosensor was 102.6%. In this sensor, the electrochemical reduction of H_2O_2 started at −0.4 V, with a peak at −0.7 V. The MXene-based biosensor has superior sensitivity compared to previous models, such as hemoglobin-glued MXene (LOD of about 20 nM for H_2O_2) and tyrosinase–MXene for phenol detection (LOD of about 12 nM). This electrochemical biosensor has a high accuracy and non-invasive approach for protein-based applications in biomedical detection and diagnostics.

A high-performance flexible piezoresistive sensor was developed in another research, using a 3D spacer textile structure coated with $Ti_3C_2T_x$-MXene nanosheets on both sides of the textile and its middle-curved fibers. It was a conductive network that was then assembled with a PDMS film and interdigital electrodes to complete the pressure-sensing device (Fig. 10A). Its DNA-like double-helix structure, reinforced with curved support fibers, creates a 3D conductive network with exceptional compressibility and durability. The sensor exhibited a speedy response time of less than 15 ms, a high sensitivity of about 35 kPa with a response range from 0 to 40 kPa, a detection

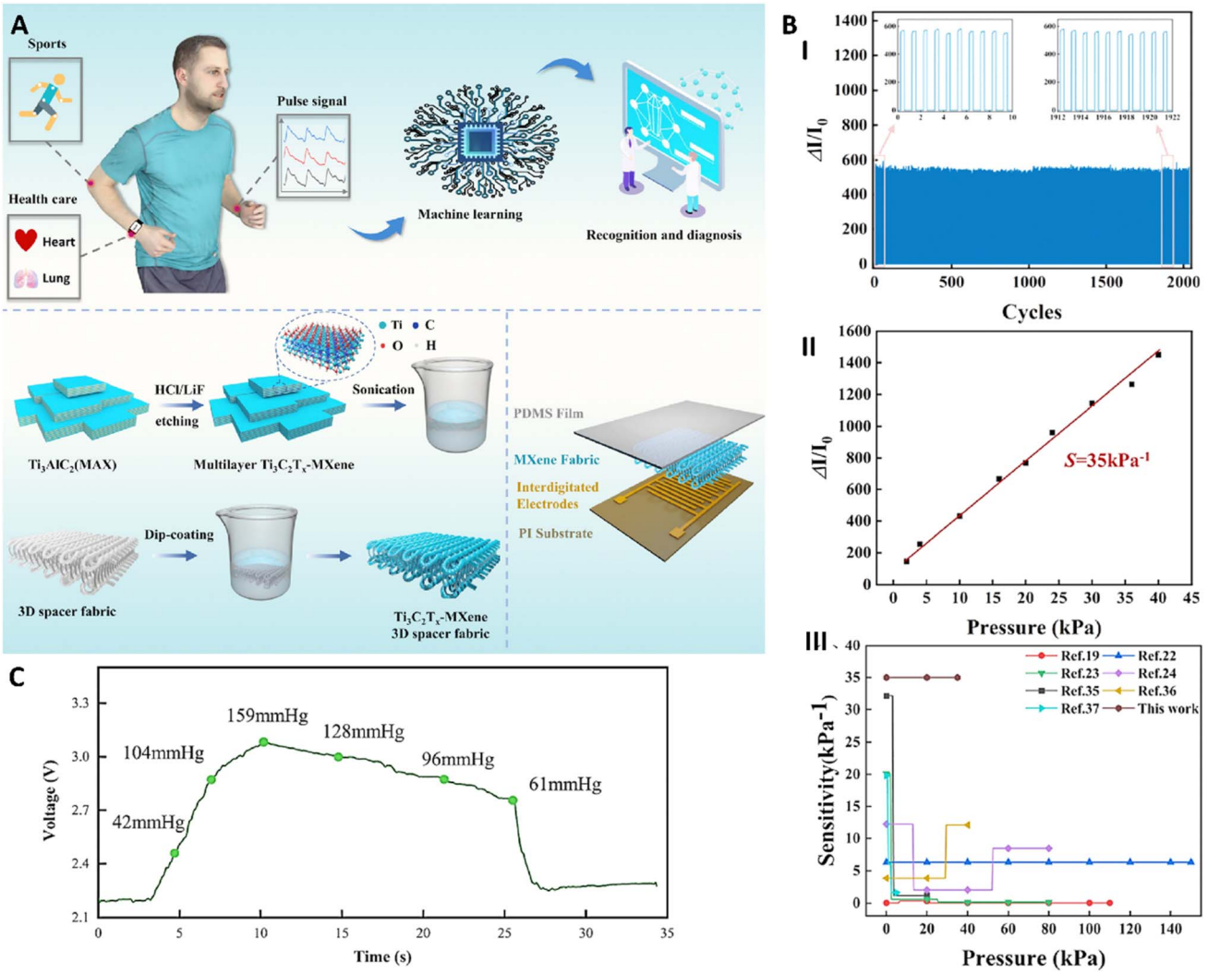

Fig. 10 (A) Schematic image related to the fabrication process and application of the MXene-spacer fabric (MSF) sensor. (B) Sensing properties measurement, assessment of stability (I) and sensitivity (II). (III) Measuring the sensitivity of the MSF. (C) Sensor results of pressure variations during blood pressure measurement. Reprinted with permission from ref. 150. Copyright 2023, Royal Society of Chemistry.

Table 1 Other recent developments of self-powered biomedical wearables with MXenes as part of their active material

Applications	Sensor type	MXene-based active material	Effect of MXene addition	Ref.
Pressure sensor (personal medical diagnosis)	Piezoresistive pressure sensor	MXene/TPU	• Increased sensor's performance • Ultrahigh sensitivity	153
Monitoring electrophysiological signals Wound healing	Piezoresistive	AgNPs/MXene/GG/Alg-PBA	• Enhanced mechanical strength • Enhanced electrical conductivity	13
Real-time human healthcare monitoring	Strain sensor	CNT/MXene/PDMS	• Perfect cycling durability • Superior temperature stability	154
Human physiological signals for medical diagnosis	Capacitive pressure sensor	MXene/PVDF-TrFE nanofiber scaffolds between PEDOT:PSS/PDMS electrodes	• Increased the dielectric constant • Reduced the compression modulus • Enhanced the sensing properties	155
Wireless monitoring	Strain sensor	MXene hydrogel (PMZn-GL)/PVA/Zn^{2+}	• Enhanced mechanical properties • Improved electrical conductivity	156
Glucose detection	Electrochemical sensor	Ti_3C_2–HF/TBA	• High selectivity and sensitivity	157
Cardiovascular health management	Strain sensor	MXene–PU mesh	• Improved conductivity and mechanical resilience • Providing breathability	158
Wound healing acceleration	Triboelectric nanogenerator	MXene/gelatin	• Increased electrical conductivity • Excellent photothermal conversion properties	109
Body monitoring Thermotherapy Electromagnetic interference shielding	Piezoresistive strain sensor	PVDF/MXene/PI	• Made conductive network for sensing and heating • Ideal mechanical properties	159
Breath monitoring	Volatile organic compounds (VOCs)	$Ti_3C_2T_x$-M2	• High electrical conductivity • Increase sensitivity	160
Monitor human movement	Strain sensor	$Ti_3C_2T_x$/PVA	• Enhanced the sensor's electrical, mechanical, and sensing properties	161
Medical diagnostics	Strain sensor	MXene/PAA	• Improved toughness and strength • Enhanced conductivity	162
Sweat-powered wearable	Hydroelectric nanogenerator (HENG)	$Ti_3C_2T_x$ MXene	• Efficient absorption of water molecules due to the hydrophilicity of MXenes • Higher performance and power density (0.683 mW cm^{-2}) compared to previous devices	163
Multi-weather triboelectric textile	TENG	MXene/cotton	• Significant stability due to MXene–cotton interactions (only 0.016% of MXene was lost after a 120 minute wash) • Enhancing electrical conductivity	164
Self-powered personal thermal management device (PTM)	TENG	$Fe_xCo_{1-x}P$ nanostructures/MXene	• Increase in the surface temperature after MXene addition • Higher thermal insulation of the device • Enhanced durability of the device	165
Multi-signal wearable sensor	TENG	Catechol-modified PVA (Pc)/MXene/poly(*N*-acryloyl glycinamide) (PNAGA) hydrogel	• MXene nanosheets retain a portion of the electrical conductivity of the device after water evaporation	166
Detection of lead ion (Pb^{2+}) in plasma	Enzyme-free biofuel capacitors	AuNPs/MXene (capacitor anode)	• Decreasing the resistance of the anode after the addition of AuNPs/MXene (from 106 to 41 Ω) • MXenes increased the sensitivity of the device by 5.76 times	167
Pressure sensor and human motion detection	Solar cell-powered supercapacitors	Black phosphorous (BP)/MXene film	• Synergic effect of MXene and BP in improving the electrical properties of the active film	168

limit of 20 Pa, ultra-fast response time of 15 ms, and excellent durability over 2000 cycles (Fig. 10B). A pulse monitoring system integrating hardware and using machine learning algorithms like random forest (RF), support vector machine (SVM), and convolutional neural network (CNN) for disease classification achieved 98.8% accuracy in identifying cardiovascular disease-

related pulse signals. This sensor can detect a wide range of body motion, such as finger bending, knee movement, and smiling. This device could be integrated into smart healthcare systems and be able to pulse analysis and cardiovascular disease detection. The MXene-spacer fabric (MSF) sensor was also capable of measuring blood pressure (Fig. 10C) with high sensitivity and stability, recording a maximum pressure of 159 mmHg. It accurately captured both systolic and diastolic pressures, comparable to standard sphygmomanometer readings. Overall, the textile-based MSF sensor can reliably monitor both weak pulse signals and stronger signals like blood pressure.[150]

An effective self-powered MXene-based smart bandage was produced in research for wound bacterial infection detection. The wearable smart bandage primarily consisted of a flexible circuit board and an electrode array. Its multilayer design, supported by a thin polyimide (PI) substrate, incorporated a microcontroller unit (MCU), an NFC chip, an integrated amplifier, an analog-to-digital converter (ADC), and a digital-to-analog converter (DAC), all assembled on the top of the circuit board. The system exhibited wide detection ranges (from 1 pg mL^{-1} to 100 ng mL^{-1} and 1 μM to 100 μM for sortase A and pyocyanin, respectively), ensuring accurate identification of two types of wound infections, *Staphylococcus aureus* and *Pseudomonas aeruginosa*. Selectivity tests confirmed that potential interfering substances, such as glucose, creatinine, uric acid, and hydrogen peroxide, had no significant impact on the signal output. Differential pulse voltammetry (DPV) was used to measure oxidation peaks with a pulse amplitude of 50 mV and a pulse width of 60 ms. The *in vivo* test with a 1.6 cm diameter wound showed 92.8–103.4% recovery rates, validating the accuracy of the smart bandage for real-time wound infection assessment. Additionally, the near-field communication (NFC) module maintained stable wireless power and data transmission within a 30 mm range, even under bending conditions, ensuring reliable operation during wear. These results highlighted the potential of this wearable, non-invasive system for real-time, high-accuracy wound infection monitoring, addressing critical challenges in personalized wound care management.[151]

Chen *et al.*,[152] developed a non-invasive wearable sweat sensor utilizing machine learning (ML) algorithms for cardiovascular disease (CVD) detection. The sensor was based on an MXene hydroxyl and silver nanowires (AgNW) composite, which enhanced sensitivity for cholesterol biomarker detection in sweat. Machine learning algorithms were integrated for sweat sample classification to improve diagnostic accuracy. The surface-enhanced Raman spectroscopy (SERS) substrate demonstrated detecting cholesterol concentrations as low as 10^{-8} M. A strong linear correlation was detected between cholesterol concentration and SERS signal intensity. Additionally, the sensor showed excellent durability, maintaining over 50 stretch-release cycles. Mechanical tests showed that the sensor retained its functionality after mechanical deformation and 18 h of continuous wear. Therefore, the combination uses of SERS and ML algorithms showed a promising method for fabrication of wearable sensors for real-time CVD detection.

Table 1 summarizes some other recent advancements in the field of MXene-based wearable devices and nanogenerators.

5 Challenges

The transformation of wearable electronics from inflexible structures to flexible, stretchy devices enhances various fields such as mobile healthcare and energy storage. There is a growing interest in MXenes due to their large surface area, enriched functionalities, and high electrical conductivity. Advancements in MXene-enabled flexible electronics emphasize nonstructural features and nanometric scale devices, including 3D configurations and diverse substrates. Applications in electromagnetic interference shielding, energy, healthcare, and humanoid machine control illustrate the promising potential of MXene nanoparticles for next-generation wearable technologies. Additionally, design challenges associated with these devices are addressed, along with proposed solutions.[9,169] While MXene-based self-powered wearable devices hold significant promise for advancing biomedical applications, several challenges and limitations must be addressed to facilitate their widespread adoption and effectiveness. These challenges span various aspects, including material properties, device performance, and integration into healthcare systems.

5.1 Long-term stability

One of the primary concerns regarding MXene-based devices is their long-term stability.[170] MXenes are susceptible to oxidation and degradation when exposed to moisture and oxygen, which can compromise their electrical performance and biocompatibility over time.[170,171] Ensuring that these materials maintain their properties in real-world conditions is crucial for the reliability and durability of wearable devices intended for continuous use. Research is needed to develop protective coatings and strategies to enhance the environmental stability of MXenes. Additionally, their preparation poses challenges, particularly because they are derived from ceramics (MAX phase) through etching, which exposes metal atoms and embeds anions and cations.[172] The resulting MXenes are often thermodynamically metastable, making them susceptible to oxidation and degradation, which significantly diminishes their activity and performance. Thus, enhancing the stability of MXenes-based materials is crucial for their practical applications. Key factors affecting stability include oxidation of MXenes flakes, the stability of colloidal solutions, and the swelling and degradation of thin films. Strategies for improving stability involve optimizing MAX phase synthesis, modifying preparation methods, and controlling storage conditions, as well as forming protective coatings on the surfaces or edges of MXenes flakes. Future developments and challenges in creating highly active and stable MXenes are also essential for advancing their design, preparation, and application in various fields.[172] Antioxidation strategies currently available to stabilize MXenes in their natural aqueous dispersion form are limited, primarily focusing on enhancing their shelf-life.[171] However, there is a need for

further investigation into the overall impact of these antioxidants on MXenes' performance across various applications. Since these strategies predominantly rely on surface capping of MXenes, systematic research is essential to comprehend the molecular interactions between antioxidants and MXenes, as well as the stereospecific orientation of the antioxidants on the MXenes surface. Additionally, concerns regarding the concentration of antioxidants and their complete removal from the MXenes surface persist. Therefore, future research should shift towards exploring more potent antioxidant molecules capable of effectively stabilizing MXenes at lower doses while ensuring ease of removal or eliminating the need for removal altogether.[171]

A major bottleneck for MXene application lies in their tendency to restack or aggregate during storage or processing, resulting in poor dispersion in aqueous or organic media. This aggregation diminishes their active surface area, electrical conductivity, and overall functional performance. Recent research has focused on strategies to overcome this limitation. For instance, the intercalation of trace metal cations (such as Li^+, Mg^{2+}, Al^{3+}) into MXene layers has proven effective. These cations act as nanoscale pillars that prevent face-to-face restacking by increasing interlayer spacing. The intercalated MXenes exhibit improved redispersion after drying, enabling better processability and longer shelf life without compromising their intrinsic properties.[173] Moreover, surface functionalization and chemical modification have been extensively explored to enhance the hydrophilicity and colloidal stability of MXenes. Incorporation of hydrophilic functional groups improves their compatibility with aqueous environments and reduces van der Waals-driven aggregation.[173–175]

MXenes are mechanically flexible yet prone to structural fatigue and degradation when subjected to repeated mechanical stress, which is inevitable in wearable devices. To address this, hybridization with other nanomaterials such as graphene, carbon nanotubes, or flexible polymers has been widely reported. These composites leverage the superior mechanical strength and elasticity of the added components while retaining the electrical and chemical advantages of MXenes.[176–180] The formation of hydrogen bonds and electrostatic interactions between MXenes and polymer matrices also plays a crucial role in enhancing mechanical resilience. This synergistic effect allows for improved tensile strength, toughness, and durability under cyclic loading, maintaining stable device performance over extended periods. Such advances in mitigating dispersion and mechanical limitations directly impact the development of MXene-based self-powered wearable devices. Stable dispersion ensures uniform composite formation and consistent electrical properties, critical for sensors and energy harvesters. Enhanced mechanical integrity guarantees device robustness during prolonged use in dynamic, real-world biomedical environments, supporting accurate and reliable health monitoring.

5.2 Energy harvesting efficiency

Although MXene-based devices can efficiently convert mechanical energy into electrical energy using technologies like triboelectric and piezoelectric generators, the overall energy harvesting efficiency remains a challenge.[181] The energy output generated from body movements may not be sufficient to power more complex sensors and devices, especially those requiring continuous operation. Improving energy conversion efficiency and exploring hybrid energy harvesting systems may help overcome this limitation. Notably, the inherent properties of MXenes, including their high conductivity and mechanical flexibility, contribute to their potential in energy harvesting applications.[182–185] However, several factors impede the overall efficiency. For instance, the interface between MXenes and the materials used in the generators can affect energy transfer, leading to energy loss. Additionally, the design and configuration of the devices play a crucial role; optimizing these aspects is essential to maximize output. Moreover, the environmental conditions under which these devices operate can significantly influence their performance. Variability in temperature, humidity, and mechanical stress can impact the stability and efficiency of energy conversion processes. Therefore, developing MXene-based devices that maintain high efficiency across a range of conditions is vital. Furthermore, enhancing the surface area and improving the contact mechanics between MXenes and other materials may lead to better energy harvesting capabilities.

5.3 Sensing modalities

MXenes, with their remarkable electrical and mechanical properties, hold promise for high-performance sensors capable of detecting a wide range of biomarkers, environmental factors, and physiological parameters.[186–189] However, developing sophisticated sensing modalities is another significant challenge for MXene-based wearable devices.[190] While MXenes can be integrated into various biosensors, achieving high sensitivity, specificity, and accuracy in detecting biomarkers is critical for reliable health monitoring and disease diagnosis.[191,192] However, creating sensors that can reliably function in dynamic real-world conditions remains a hurdle. Furthermore, the integration of multiple sensing modalities into a single device complicates the design and fabrication process. For instance, combining sensors that detect glucose levels, heart rate, and temperature require careful engineering to ensure that each sensor operates effectively without interference from the others. This complexity demands innovative strategies in materials science and engineering. Additionally, the need for miniaturization cannot be overstated. Wearable devices must be lightweight and comfortable for users, which necessitates the development of compact sensing technologies that do not compromise performance. Achieving this balance between size and functionality is a critical challenge for researchers. Moreover, the longevity and stability of the sensors under various environmental conditions are vital. MXene-based sensors must maintain their performance over time and withstand factors such as humidity, temperature variations, and exposure to different chemicals. Ensuring durability while retaining sensitivity is a key area of focus. Notably, the incorporation of signal processing and data interpretation algorithms is essential to

convert raw sensor data into meaningful health insights. Developing sophisticated algorithms that can interpret complex data accurately and provide users with actionable information adds another layer of complexity to the design of MXene-based wearable devices. The need for mediator-free biosensors poses additional challenges in ensuring effective electron transfer between bioreceptors and electrodes. Continued research into optimizing sensor designs and enhancing the interaction between MXenes and biomolecules is essential.

5.4 Biocompatibility and cytotoxicity

While MXenes and their composites have demonstrated promising biocompatibility for various biomedical applications, it is important to acknowledge that findings are not uniformly positive. Recent studies indicate that biocompatibility can vary significantly depending on factors such as MXene composition, surface functionalization, flake size, dosage, and exposure duration. Some reports highlight potential cytotoxicity and immunogenic responses under certain conditions, underscoring the complexity of MXene–biological interactions. Moreover, comprehensive long-term toxicity and immunological assessments remain limited, emphasizing the need for standardized, in-depth studies to fully understand their safety profile. Thus, although MXenes offer great potential, caution and rigorous evaluation are essential before their widespread clinical adoption.[193–195] Understanding the long-term effects of MXene exposure on human tissues is crucial for their acceptance in healthcare settings.[195,196] For instance, titanium (Ti)-based MXenes, particularly $Ti_3C_2T_x$, have been extensively studied for biomedical applications; however, they exhibit limitations such as low biocompatibility and potential disruption of spermatogenesis, along with accumulation in the uterus. In contrast, non-Ti MXenes are emerging as promising alternatives due to their superior biodegradability and enhanced biocompatibility.[197] These non-Ti MXenes are being explored for various applications, including drug delivery, photothermal therapy, chemodynamic therapy, and sonodynamic therapy. Some also demonstrate enzyme-mimicking activity, aiding in the scavenging of reactive oxygen species (ROS). Significant properties of non-Ti MXenes include their biocompatibility, biodegradability, antibacterial activity, and neuroprotective effects, which are crucial for managing chronic diseases. Additionally, their theranostic applications include roles as nanozymes for sensing and therapeutic purposes, along with an examination of their antibacterial properties and underlying mechanisms. Thus, non-Ti MXenes present unique properties and potential challenges in the biomedical field.[197] Notably, to enhance biocompatibility, bioactive materials can be applied to modify the surface of MXenes, enabling the design of multifunctional MXene-based nanomaterials tailored for various biomedical applications, ultimately achieving improved therapeutic effects and more desirable biological functions.[198]

5.5 Integration with emerging technologies

The successful integration of MXene-based wearable devices with emerging technologies, such as AI and the IoT, presents both opportunities and challenges.[199,200] While these integrations can enhance the functionality and user experience of wearable devices, they also require efficient data management and communication protocols. Ensuring data security and privacy is paramount in healthcare applications, necessitating robust cybersecurity measures. On one hand, the incorporation of AI can significantly enhance the functionality of wearable devices. By leveraging machine learning algorithms, these devices can analyze real-time data, providing users with personalized health insights and predictive analytics. This capability can lead to improved health monitoring and more proactive healthcare management, making MXene-based wearables not just passive monitors but active participants in the user's health journey. Moreover, the IoT facilitates seamless communication between wearable devices and other connected systems, enabling a holistic approach to health management. For instance, data collected from MXene-based wearables can be transmitted to healthcare providers, allowing for continuous monitoring and timely interventions. This interconnectedness enhances the user experience by enabling a more integrated and responsive healthcare ecosystem. However, these advancements come with challenges, particularly in data management and communication protocols. Efficiently handling the vast amounts of data generated by wearable devices is crucial. This requires robust data processing capabilities and streamlines communication systems to ensure information is conveyed accurately and promptly.

6 Future directions

As the field of MXene-based self-powered wearable devices advances, targeted strategies are needed to overcome current limitations and unlock their full biomedical potential. One concrete direction involves enhancing energy harvesting efficiency through the development of hybrid systems that integrate triboelectric, piezoelectric, and thermoelectric mechanisms within a single wearable platform. For instance, designing multilayered MXene composites combined with flexible substrates can maximize energy capture from diverse physiological movements and temperature gradients, enabling continuous, autonomous device operation. Beyond improving energy harvesting efficiency, future developments should focus on scalable and environmentally friendly MXene synthesis methods to lower costs and facilitate mass production. For example, greener etching processes and precursor reuse can reduce toxic byproducts and financial barriers, accelerating commercial viability.

In sensing technology, the functionalization of MXenes with tailored nanomaterials such as graphene, conducting polymers, and enzyme-mimetic molecules can significantly boost sensitivity and selectivity towards specific biomarkers. Employing advanced fabrication techniques like 3D printing and microfluidic patterning allows the creation of intricately structured, customizable sensors that conform precisely to target biomedical applications, thereby enabling personalized health monitoring with improved accuracy. The next step involves

engineering MXene-based multimode sensors capable of independently detecting multiple stimuli (pressure, temperature, chemical markers) simultaneously. This can be achieved by designing MXene composites with porous 3D architectures and coupling them with advanced signal decoupling algorithms powered by machine learning. Such multifunctional sensors, integrated *via* high-precision printing methods, will offer compact, low-cost platforms for comprehensive health monitoring. Material innovation should continue in the direction of bio-inspired and self-healing MXene composites. Incorporating dynamic covalent bonds or reversible crosslinking chemistries will enable hydrogels or elastomers containing MXenes to autonomously repair mechanical damage, extending device lifespan and reliability critical for wearable applications. Furthermore, the development of MXene-based smart contact lenses demonstrates promising application-specific future devices. These lenses integrate real-time biosensing with drug delivery and ocular therapy capabilities, illustrating how MXene's flexibility and conductivity can be harnessed for minimally invasive health monitoring.

Moreover, embedding artificial intelligence (AI) and machine learning algorithms directly into the device firmware presents a transformative opportunity for real-time physiological data analysis and decision-making. This integration can facilitate early detection of anomalies, predictive health risk assessments, and individualized treatment recommendations. To realize this, development efforts should focus on optimizing low-power, edge-computing-compatible AI models tailored for wearable resource constraints. The integration of MXene-based wearable devices with wireless communication modules (Bluetooth, NFC) and energy storage units (flexible supercapacitors, solid-state batteries) is essential for creating fully autonomous systems. Strategies like embedding MXenes in flexible electrodes for these energy storage devices combine high conductivity and mechanical resilience, providing stable power sources for continuous operation.

Addressing biocompatibility and user comfort remains paramount. Innovations in surface engineering of MXenes to enhance skin compatibility, reduce immune response, and improve mechanical durability are critical. Incorporating stretchable and breathable designs using elastomeric composites ensures devices conform naturally to body contours, promoting long-term wearability and user compliance. Coating MXene surfaces with biocompatible polymers or zwitterionic materials can mitigate immune responses and oxidation, improving skin-friendliness and device durability. Coupled with ergonomic designs incorporating breathable, stretchable substrates and adhesive interfaces, these advances will ensure sustained user comfort and acceptance.

Overall, MXene-based wearables hold significant promise for disease diagnostics and therapy. The development of biosensors capable of multiplexed biomarker detection in sweat and interstitial fluid can facilitate early cancer and chronic disease diagnosis. Concurrently, harnessing MXenes' photothermal properties offers avenues for localized therapeutic interventions coupled with real-time treatment monitoring. The convergence of material innovation, device engineering, and AI-powered analytics thus defines a clear roadmap towards next-generation, clinically impactful MXene wearable technologies.

7 Conclusion

The biomedical potential of MXene-based self-powered wearable devices is not merely a technological advancement; it represents a paradigm shift in how we approach health monitoring and disease management. The unique properties of MXenes—such as their exceptional electrical conductivity, biocompatibility, hydrophilicity, and large surface area—position them as ideal candidates for powering innovative biosensors and wearable technologies. These devices enable continuous and non-invasive monitoring of vital signs and biomarkers, which can significantly enhance patient care by providing real-time data. This capability allows for a more proactive approach to health management, empowering individuals to make informed decisions about their wellness and facilitating timely interventions by healthcare providers. Moreover, the integration of MXenes with advanced energy harvesting technologies addresses a critical barrier often faced in wearable devices: the dependency on external power sources. By utilizing mechanical energy from body movements or thermal energy from body heat, MXene-based devices can operate autonomously, thereby extending their usability and convenience. This independence from traditional power sources not only enhances the practicality of wearable devices but also opens new avenues for their application in remote and resource-limited settings, where access to electricity may be a challenge. As research progresses in optimizing the energy harvesting efficiency and durability of MXene-based devices, we can anticipate a future where these technologies become ubiquitous in everyday health monitoring. The potential for these devices to be used in personalized medicine, particularly in the detection and management of chronic diseases like cancer and diabetes, underscores their significance in modern healthcare. However, the road ahead is not without challenges that require critical thinking and innovative solutions. Issues related to the long-term stability of MXenes, the need for sophisticated sensing modalities, and biocompatibility must be rigorously addressed to ensure the safety and effectiveness of these devices in clinical applications. Furthermore, as MXene-based wearable technologies become more integrated into healthcare systems, considerations regarding data privacy, security, and the ethical implications of constant health monitoring will become increasingly important. Engaging in interdisciplinary research that encompasses material science, engineering, healthcare, and ethics will be essential for realizing the full potential of MXene-based self-powered wearable devices. By addressing these challenges thoughtfully, we can utilize the full capabilities of these technologies, ultimately transforming the landscape of personalized medicine and enhancing the quality of care for patients worldwide.

Author contributions

Y. M. S.: writing original draft – review & editing; S. L.: writing original draft – review & editing; M. E.: writing original draft –

review & editing; A. Z: writing – review & editing; A. K.: visualization, writing – review & editing; S. I.: supervision, conceptualization, writing original draft – review & editing; A. Z.: supervision, review & editing.

Conflicts of interest

Author(s) declare no conflict of interest.

Data availability

No primary research results, software or code have been included, and no new data were generated or analysed as part of this review.

References

1 R. C. Reid and I. Mahbub, *Curr. Opin. Electrochem.*, 2020, **19**, 55–62.
2 Y. Song, D. Mukasa, H. Zhang and W. Gao, *Acc. Mater. Res.*, 2021, **2**, 184–197.
3 G. Vulpe, G. Liu, S. Oakley, D. Pletsas, G. Yang, R. Dutra, O. Guy, Y. Liu, M. Waldron, J. Neary, A. A. Mohan and S. Sharma, *Biosens. Bioelectron.:X*, 2024, **19**, 100500.
4 W. Fu, B. Yu, D. Ji, Z. Zhou, X. Li, R. Wang, W. Lu, Y. Sun and Y. Dai, *Responsive Mater.*, 2024, **2**(4), e20240018.
5 Y. Zhang, Y. Hu, N. Jiang and A. K. Yetisen, *Biosens. Bioelectron.*, 2023, **219**, 114825.
6 Y. Zou, L. Bo and Z. Li, *Fundam. Res.*, 2021, **1**, 364–382.
7 D. Macário, I. Domingos, N. Carvalho, P. Pinho and H. Alves, *iScience*, 2022, **25**, 103977.
8 M. Parrilla and K. De Wael, *Adv. Funct. Mater.*, 2021, **31**, 2107042.
9 J. Ma, K. Yang, Y. Jiang, L. Shen, H. Ma, Z. Cui, Y. Du, J. Lin, J. Liu and N. Zhu, *Cell Rep. Phys. Sci.*, 2022, **3**, 100908.
10 Q. Yi, X. Pei, P. Das, H. Qin, S. W. Lee and R. Esfandyarpour, *Nano Energy*, 2022, **101**, 107511.
11 A. Khosravi, A. Zarepour, A. Zarrabi and S. Iravani, *Nano-Micro Lett.*, 2026, **18**, 1–19.
12 C. Ma, M. G. Ma, C. Si, X. X. Ji and P. Wan, *Adv. Funct. Mater.*, 2021, **31**, 2009524.
13 M. Li, Y. Zhang, L. Lian, K. Liu, M. Lu, Y. Chen, L. Zhang, X. Zhang and P. Wan, *Adv. Funct. Mater.*, 2022, **32**, 2208141.
14 C. Ma, M.-G. Ma, C. Si, X.-X. Ji and P. Wan, *Adv. Funct. Mater.*, 2021, **31**, 2009524.
15 Y. Ren, Q. He, T. Xu, W. Zhang, Z. Peng and B. Meng, *Biosensors*, 2023, **13**, 495.
16 S. Iravani and R. S. Varma, *Mater. Adv.*, 2023, **4**, 4317–4332.
17 S. Abdulmalek, A. Nasir, W. A. Jabbar, M. A. M. Almuhaya, A. K. Bairagi, M. A. M. Khan and S. H. Kee, *Healthcare*, 2022, **10**, 1993.
18 A. I. Paganelli, A. G. Mondéjar, A. Cardoso da Silva, G. Silva-Calpa, M. F. Teixeira, F. Carvalho, A. Raposo and M. Endler, *J. Biomed. Inf.*, 2022, **127**, 104009.
19 Y. Song, J. Xu, X. Xiao, F. Manshaii, Y. Wang, J. Tang, L. Huang and J. Chen, *Mater. Today*, 2025, **87**, 304–328.
20 Y. Zou, L. Bo and Z. Li, *Fundam. Res.*, 2021, **1**, 364–382.
21 C. Liu, Z. Feng, T. Yin, T. Wan, P. Guan, M. Li, L. Hu, C. H. Lin, Z. Han, H. Xu, W. Chen, T. Wu, G. Liu, Y. Zhou, S. Peng, C. Wang and D. Chu, *Adv. Mater.*, 2024, **36**, 2403791.
22 W. Lin, Y. Wei, X. Wang, K. Zhai and X. Ji, *Machines*, 2023, **11**, 977.
23 Y. Wang, T. Li, Y. Li, R. Yang and G. Zhang, *Biosensors*, 2022, **12**, 936.
24 H. Chenani, M. Saeidi and A. Simchi, *Prog. Mol. Biol. Transl. Sci.*, 2025, **215**, 63–99.
25 S. Tian, M. Wang, P. Fornasiero, X. Yang, S. Ramakrishna, S.-H. Ho and F. Li, *Chin. Chem. Lett.*, 2023, **34**, 108241.
26 K. Wang, W. Liu, J. Wu, H. Li, H. Peng, J. Zhang, K. Ding, X. Wang, C. Hou, H. Zhang and Y. Luo, *ACS Appl. Mater. Interfaces*, 2025, **17**, 13279–13301.
27 Y. Qiao, L. Qiao, Z. Chen, B. Liu, L. Gao and L. Zhang, *Chemosensors*, 2022, **10**, 273.
28 A. M. Amani, H. Kamyab, E. Vafa, A. Jahanbin, M. Abbasi, A. Vaez, G. Munuswamy-Ramanujam, B. Ravindran, L. Gnanasekaran, D. Rocchio and M. Yusuf, *Adv. Compos. Hybrid Mater.*, 2024, **8**, 63.
29 M. Kang and W.-H. Yeo, *Micromachines*, 2024, **15**, 884.
30 Y. Zou, L. Bo and Z. Li, *Fundam. Res.*, 2021, **1**, 364–382.
31 X. Dong, F. Liu, L. Wang, L. Xu, H. Pan and J. Qi, *Mater. Today Commun.*, 2023, **35**, 105493.
32 R. Chen, X. Jia, H. Zhou, S. Ren, D. Han, S. Li and Z. Gao, *Mater. Today*, 2024, **75**, 359–385.
33 Y. Wang, T. Guo, Z. Tian, K. Bibi, Y. Z. Zhang and H. N. Alshareef, *Adv. Mater.*, 2022, **34**(21), 2108560.
34 L. Liu, J. Yang, H. Zhang, J. Ma, J. Zheng and C. Wang, *Mater. Today Commun.*, 2023, **35**, 106014.
35 S. Sreenilayam, I. Ahad, V. Nicolosi and D. Brabazon, *Mater. Today*, 2021, **43**, 99–131.
36 W. Meng, X. Liu, H. Song, Y. Xie, X. Shi, M. Dargusch, Z.-G. Chen, Z. Tang and S. Lu, *Nano Today*, 2021, **40**, 101273.
37 S. Deng, W. Akram, X. Ye, L. Zhang, Y. Yang, S. Cheng and J. Fang, *Small*, 2024, **20**, 2404872.
38 Y. Dong, S. S. K. Mallineni, K. Maleski, H. Behlow, V. N. Mochalin, A. M. Rao, Y. Gogotsi and R. Podila, *Nano Energy*, 2018, **44**, 103–110.
39 R. Mohan and F. Ali, *Polym. Adv. Technol.*, 2023, **34**(10), 3193–3209.
40 X. Luo, L. Zhu, Y.-C. Wang, J. Li, J. Nie and Z. L. Wang, *Adv. Funct. Mater.*, 2021, **31**, 2104928.
41 M. T. Rahman, S. M. S. Rana, M. Salauddin, M. A. Zahed, S. Lee, E.-S. Yoon and J. Y. Park, *Nano Energy*, 2022, **100**, 107454.
42 C. Jiang, X. Li, Y. Yao, L. Lan, Y. Shao, F. Zhao, Y. Ying and J. Ping, *Nano Energy*, 2019, **66**, 104121.
43 W. He, M. Sohn, R. Ma and D. J. Kang, *Nano Energy*, 2020, **78**, 105383.
44 N. Sezer and M. Koç, *Nano Energy*, 2021, **80**, 105567.
45 G. Khandelwal, S. Deswal, D. Shakthivel and R. Dahiya, *J. Phys.: Energy*, 2023, **5**, 032001.
46 D. Tan, C. Jiang, N. Sun, J. Huang, Z. Zhang, Q. Zhang, J. Bu, S. Bi, Q. Guo and J. Song, *Nano Energy*, 2021, **90**, 106528.

47 Y. Guo, M. Zhong, Z. Fang, P. Wan and G. Yu, *Nano Lett.*, 2019, **19**(2), 1143–1150.
48 L. Wang, M. Tian, Y. Zhang, F. Sun, X. Qi, Y. Liu and L. Qu, *J. Mater. Sci.*, 2020, **55**, 6187–6194.
49 L. Li, J. Pan, L. Chang, Z. Liu, G. Wu and Y. Hu, *Chem. Eng. J.*, 2024, **482**, 148988.
50 Z. Cao, Y. Yang, Y. Zheng, W. Wu, F. Xu, R. Wang and J. Sun, *J. Mater. Chem. A*, 2019, **7**(44), 25314–25323.
51 F. Li, Y. Liu, S. Xinlei, H. Li, C. Wang, Q. Zhang, R. Ma and J. Liang, *Nano Lett.*, 2020, **20**(8), 6176–6184.
52 B. Peng, F. Zhao, J. Ping and Y. Ying, *Small*, 2020, **16**, 2002681.
53 L. Xie, Z. Zhang, Q. Wu, Z. Gao, G. Mi, R. Wang, H.-b. Sun, Y. Zhao and Y. Du, *Nanoscale*, 2023, **15**, 405–433.
54 S. Kizhepat, A. S. Rasal, J.-Y. Chang and H.-F. Wu, *Nanomaterials*, 2023, **13**, 1520.
55 Y. Bai, T. Xu and X. Zhang, *Micromachines*, 2020, **11**, 60.
56 S. Ozbey, G. Keles and S. Kurbanoglu, *Microchim. Acta*, 2025, **192**, 290.
57 D. Mahalakshmi, J. Nandhini, G. Meenaloshini, E. Karthikeyan, K. Karthik, J. Sujaritha and C. Ragavendran, *Nano TransMed*, 2025, **4**, 100073.
58 J. Song, Y. Luo, Z. Hao, M. Qu, C. Huang, Z. Wang, J. Yang, Q. Liang, Y. Jia and Q. Song, *Mater. Today Bio*, 2025, **32**, 101667.
59 A. Baruah, R. Newar, S. Das, N. Kalita, M. Nath, P. Ghosh, S. Chinnam, H. Sarma and M. Narayan, *Discover Nano*, 2024, **19**, 103.
60 C.-L. Lai, A. Mukundan, R. Karmakar, R. Kaur, K.-L. Huang and H.-C. Wang, *Biosensors*, 2025, **15**, 371.
61 S. Bharti, S. Tripathi and K. Singh, *Anal. Biochem.*, 2024, **685**, 115404.
62 C. Mousty and H. Farhat, *Electroanalysis*, 2023, **35**, e202200527.
63 L. Li, I. Soyhan, E. Warszawik and P. van Rijn, *Adv. Sci.*, 2024, **11**, 2306035.
64 T. Dutta, P. Alam and S. K. Mishra, *J. Mater. Chem. B*, 2025, **13**, 4279–4312.
65 X. Li, Z. Huang, C. E. Shuck, G. Liang, Y. Gogotsi and C. Zhi, *Nat. Rev. Chem.*, 2022, **6**, 389–404.
66 H. Li, R. Fan, B. Zou, J. Yan, Q. Shi and G. Guo, *J. Nanobiotechnol.*, 2023, **21**, 73.
67 S. N. Sankar, G. Araujo, J. Fernandes, F. Cerqueira, P. Alpuim, A. R. Ribeiro, F. Lebre, E. Alfaro-Moreno, E. Placidi and S. Marras, *Adv. Mater. Interfaces*, 2024, **11**, 2400203.
68 L. Zhang, W. Song, H. Liu, H. Ding, Y. Yan and R. Chen, *Processes*, 2022, **10**, 1744.
69 M. Tang, J. Li, Y. Wang, W. Han, S. Xu, M. Lu, W. Zhang and H. Li, *Symmetry*, 2022, **14**, 2232.
70 Y. Wang, T. Guo, Z. Tian, K. Bibi, Y.-Z. Zhang and H. N. Alshareef, *Adv. Mater.*, 2022, **34**, 2108560.
71 H. Vojoudi and M. Soroush, *Adv. Healthcare Mater.*, 2025, **14**, 2500359.
72 T. Wu, P. R. Kent, Y. Gogotsi and D.-e. Jiang, *Chem. Mater.*, 2022, **34**, 4975–4982.
73 T. Shimura, S. Sato, P. Zalar and N. Matsuhisa, *Adv. Electron. Mater.*, 2023, **9**, 2200512.
74 S. Pillai, A. Upadhyay, D. Sayson, B. H. Nguyen and S. D. Tran, *Molecules*, 2021, **27**, 165.
75 M. Hassan, G. Abbas, N. Li, A. Afzal, Z. Haider, S. Ahmed, X. Xu, C. Pan and Z. Peng, *Adv. Mater. Technol.*, 2022, **7**, 2100773.
76 S. Li, Y. Cong and J. Fu, *J. Mater. Chem. B*, 2021, **9**, 4423–4443.
77 H. Zheng, M. Chen, Y. Sun and B. Zuo, *Chem. Eng. J.*, 2022, **446**, 136931.
78 H. C. Ates, P. Q. Nguyen, L. Gonzalez-Macia, E. Morales-Narváez, F. Güder, J. J. Collins and C. Dincer, *Nat. Rev. Mater.*, 2022, **7**, 887–907.
79 D. Wang, S. Ren, J. Chen, Y. Li, Z. Wang, J. Xu, X. Jia and J. Fu, *Chem. Eng. J.*, 2022, **430**, 133163.
80 Y. Wang, W. Zhu, Y. Deng, B. Fu, P. Zhu, Y. Yu, J. Li and J. Guo, *Nano Energy*, 2020, **73**, 104773.
81 Q.-h. Lin, S. He, Q.-q. Liu, J.-h. Yang, X.-d. Qi and Y. Wang, *Compos. Sci. Technol.*, 2022, **226**, 109528.
82 S. Zhang, C. Ge and R. Liu, *Sens. Actuators, A*, 2022, **341**, 113580.
83 Y. Zhang, M. Gong and P. Wan, *Matter*, 2021, **4**, 2655–2658.
84 S. J. M. Yazdi and J. Baqersad, *J. Biomech.*, 2022, **130**, 110864.
85 P. Rahmani and A. Shojaei, *Adv. Colloid Interface Sci.*, 2021, **298**, 102553.
86 L. Wang, T. Xu and X. Zhang, *TrAC, Trends Anal. Chem.*, 2021, **134**, 116130.
87 S. Tang, Z. Liu and X. Xiang, *Carbon Lett.*, 2022, **32**, 1395–1410.
88 Y. Zheng, J. Wang, T. Cui, J. Zhu and Z. Gui, *J. Colloid Interface Sci.*, 2024, **653**, 56–66.
89 K. Ou, M. Wang, C. Meng, K. Guo, N. S. Emon, J. Li, K. Qi, Y. Dai and B. Wang, *Compos. Sci. Technol.*, 2024, **255**, 110732.
90 G. N. Islam, A. Ali and S. Collie, *Cellulose*, 2020, **27**, 6103–6131.
91 S. M. A. Mokhtar, E. Alvarez de Eulate, M. Yamada, T. W. Prow and D. R. Evans, *Med. Devices Sens.*, 2021, **4**, e10160.
92 D. Liu, C. Huyan, Z. Wang, Z. Guo, X. Zhang, H. Torun, D. Mulvihill, B. B. Xu and F. Chen, *Mater. Horiz.*, 2023, **10**, 2800–2823.
93 K. Zhou, K. Dai, C. Liu and C. Shen, *SmartMat*, 2020, **1**, e1010.
94 S. Zhang, Z. He, W. Zhao, C. Liu, S. Zhou, O. O. Ibrahim, C. Wang and Q. Wang, *Nanomaterials*, 2024, **14**, 857.
95 S. Kummari, L. R. Panicker, J. Rao Bommi, S. Karingula, V. Sunil Kumar, K. Mahato and K. Y. Goud, *Biosensors*, 2023, **13**, 420.
96 S. Larijani, A. Zarepour, A. Khosravi, S. Iravani, M. Eskandari and A. Zarrabi, *J. Mater. Chem. A*, 2025, **13**, 158–183.
97 Y. Gao, M. Rezaie and S. Choi, *Nano Energy*, 2022, **104**, 107923.
98 R. Ma, L. Cao, J. Zhuo, J. Lu, J. Chen, J. Huang, G. Yang and F. Yi, *Adv. Energy Mater.*, 2023, **13**, 2301219.

99 Y. Zhu, J. Ma, P. Das, S. Wang and Z. S. Wu, *Small Methods*, 2023, **7**, 2201609.
100 Q. Fan, M. Chen, Y. Yang, S. Wang, Y. Chen, L. Jiang, Z. Wu, P. Yu, K. Chen and F. Ge, *Adv. Mater.*, 2025, **37**(34), 2505584.
101 C. Liu, Z. Feng, T. Yin, T. Wan, P. Guan, M. Li, L. Hu, C. H. Lin, Z. Han, H. Xu, W. Cheng, T. Wu, G. Liu, Y. Zhou, S. Peng, C. Wang and D. Chu, *Adv. Mater.*, 2024, **36**, e2403791.
102 C. Liu, Z. Feng, T. Yin, T. Wan, P. Guan, M. Li, L. Hu, C.-H. Lin, Z. Han, H. Xu, W. Cheng, T. Wu, G. Liu, Y. Zhou, S. Peng, C. Wang and D. Chu, *Adv. Mater.*, 2024, **36**, 2403791.
103 L. Jia, S. Zhou, A. Ahmed, Z. Yang, S. Liu, H. Wang, F. Li, M. Zhang, Y. Zhang and L. Sun, *Chem. Eng. J.*, 2023, **475**, 146361.
104 Y. Tian, Y. An and B. Xu, *Nano Energy*, 2022, **101**, 107556.
105 S. Ghorbanzadeh and W. Zhang, *Nano Energy*, 2024, **125**, 109558.
106 J. San Nah, S. C. Barman, M. A. Zahed, M. Sharifuzzaman, H. Yoon, C. Park, S. Yoon, S. Zhang and J. Y. Park, *Sens. Actuators, B*, 2021, **329**, 129206.
107 M. Salauddin, S. S. Rana, M. T. Rahman, M. Sharifuzzaman, P. Maharjan, T. Bhatta, H. Cho, S. H. Lee, C. Park and K. Shrestha, *Adv. Funct. Mater.*, 2022, **32**, 2107143.
108 Y. Feng, H. Liu, W. Zhu, L. Guan, X. Yang, A. V. Zvyagin, Y. Zhao, C. Shen, B. Yang and Q. Lin, *Adv. Funct. Mater.*, 2021, **31**, 2105264.
109 M. Mao, J. Kong, X. Ge, Y. Sun, H. Yu, J. Liu, W. Huang, D. Y. Wang and Y. Wang, *Chem. Eng. J.*, 2024, **482**, 148949.
110 L. Yang, C. Liu, W. Yuan, C. Meng, A. Dutta, X. Chen, L. Guo, G. Niu and H. Cheng, *Nano Energy*, 2022, **103**, 107807.
111 Z. Zhang, Q. Yan, Z. Liu, X. Zhao, Z. Wang, J. Sun, Z. L. Wang, R. Wang and L. Li, *Nano Energy*, 2021, **88**, 106257.
112 L. X. Liu, W. Chen, H. B. Zhang, Q. W. Wang, F. Guan and Z. Z. Yu, *Adv. Funct. Mater.*, 2019, **29**, 1905197.
113 X. Yang, F. Wu, C. Xu, L. Yang and S. Yin, *J. Alloys Compd.*, 2022, **928**, 167137.
114 S. Zhang, A. Chhetry, M. A. Zahed, S. Sharma, C. Park, S. Yoon and J. Y. Park, *npj Flexible Electron.*, 2022, **6**, 11.
115 M. L. Matias, C. Pereira, H. V. Almeida, S. Jana, S. Panigrahi, U. D. Menda, D. Nunes, E. Fortunato, R. Martins and S. Nandy, *Mater. Today Adv.*, 2024, **23**, 100512.
116 M. Greaves, M. Mende, J. Wang, W. Yang and S. Barg, *J. Mater. Res.*, 2021, 1–23.
117 Z. Fan, C. Wei, L. Yu, Z. Xia, J. Cai, Z. Tian, G. Zou, S. X. Dou and J. Sun, *ACS Nano*, 2020, **14**, 867–876.
118 Y. Kim, E. Kim, D. Kim, C. W. Ahn, B. S. Kim, K. H. Ahn, Y. Lee and J. D. Park, *Korea Aust. Rheol. J.*, 2023, **35**, 117–125.
119 Z. Fan, J. Jin, C. Li, J. Cai, C. Wei, Y. Shao, G. Zou and J. Sun, *ACS Nano*, 2021, **15**, 3098–3107.
120 X. Li, S. Wang, M. Zheng, Z. Ma, Y. Chen, L. Deng, F. Guang, S. Khademolqorani, S. N. Banitaba and A. I. Osman, *Nanoscale Horiz.*, 2024, **9**(10), 1703–1724.
121 M. Zhang, Z. Tan, Q. Zhang, Y. Shen, X. Mao, L. Wei, R. Sun, F. Zhou and C. Liu, *ACS Appl. Mater. Interfaces*, 2023, **15**, 30849–30858.
122 J. Huang, Y. Hao, M. Zhao, W. Li, F. Huang and Q. Wei, *ACS Appl. Mater. Interfaces*, 2021, **13**, 24774–24784.
123 T. Bhatta, P. Maharjan, H. Cho, C. Park, S. H. Yoon, S. Sharma, M. Salauddin, M. T. Rahman, S. S. Rana and J. Y. Park, *Nano Energy*, 2021, **81**, 105670.
124 A. Hamzehlouy, M. Tavakoli Dare, F. Shahi, E. A. Dawi and H. A. Khonakdar, *Polym. Adv. Technol.*, 2024, **35**, e70008.
125 Y. Long, Z. Wang, F. Xu, B. Jiang, J. Xiao, J. Yang, Z. L. Wang and W. Hu, *Small*, 2022, **18**, 2203956.
126 Y. Ding, L.-Z. Huang, X.-X. Ji and M.-G. Ma, *Int. J. Biol. Macromol.*, 2024, **284**, 138106.
127 A. Levitt, J. Zhang, G. Dion, Y. Gogotsi and J. M. Razal, *Adv. Funct. Mater.*, 2020, **30**, 2000739.
128 P. Salles, E. Quain, N. Kurra, A. Sarycheva and Y. Gogotsi, *Small*, 2018, **14**, 1802864.
129 L. Yao, L. Qian, W. Song, S. Zhang, Y. Zhang, L. Zhang, X. Li, G. Yan and V. Nica, *ACS Appl. Mater. Interfaces*, 2024, **16**, 48147–48162.
130 W. Cao, J. Nie, Y. Cao, C. Gao, M. Wang, W. Wang, X. Lu, X. Ma and P. Zhong, *Chem. Eng. J.*, 2024, **496**, 154097.
131 H.-w. Zhang, X. Xu, M.-l. Huang, Y.-s. Wang, Z.-q. Xu, Z.-s. Feng, Y. Zhang and Y. Wang, *Chem. Eng. J.*, 2024, **495**, 153343.
132 C. E. Shuck, K. Ventura-Martinez, A. Goad, S. Uzun, M. Shekhirev and Y. Gogotsi, *ACS Chem. Health Saf.*, 2021, **28**, 326–338.
133 J. Ma, K. Yang, Y. Jiang, L. Shen, H. Ma, Z. Cui, Y. Du, J. Lin, J. Liu and N. Zhu, *Cell Rep. Phys. Sci.*, 2022, **3**(6), 100908.
134 S. Khalid, I. Raouf, A. Khan, N. Kim and H. S. Kim, *International Journal of Precision Engineering and Manufacturing-Green Technology*, 2019, **6**, 821–851.
135 G. Rong, Y. Zheng and M. Sawan, *Sensors*, 2021, **21**, 3806.
136 K. Liu, Z. Zhao, S. Zheng, A. Liu, Y. Wang, L. Chen and Q. Miao, *Biomacromolecules*, 2024, **25**(7), 4384–4393.
137 Y. He, Z. Deng, Y. J. Wang, Y. Zhao and L. Chen, *Carbohydr. Polym.*, 2022, **291**, 119572.
138 Q. Yi, X. Pei, P. Das, H. Qin, S. W. Lee and R. Esfandyarpour, *Nano Energy*, 2022, **101**, 107511.
139 S. Lee, D. H. Ho, J. Jekal, S. Y. Cho, Y. J. Choi, S. Oh, Y. Y. Choi, T. Lee, K.-I. Jang and J. H. Cho, *Nat. Commun.*, 2024, **15**, 5974.
140 M. Ankitha, A. M. Arjun, N. Shabana and P. A. Rasheed, *Biomed. Mater. & Devices*, 2023, **1**, 339–350.
141 A. Zamhuri, G. P. Lim, N. L. Ma, K. S. Tee and C. F. Soon, *Biomed. Eng. Online*, 2021, **20**, 33.
142 Y. Lei, W. Zhao, Y. Zhang, Q. Jiang, J. H. He, A. J. Baeumner, O. S. Wolfbeis, Z. L. Wang, K. N. Salama and H. N. Alshareef, *Small*, 2019, **15**, 1901190.
143 J. V. Vaghasiya, C. C. Mayorga-Martinez, J. Vyskočil and M. Pumera, *Biosens. Bioelectron.*, 2022, **205**, 114092.
144 G. Ji, J. Wang, Z. Wang, S. Zhang, Z. Fang, Y. Wang and Z. Gao, *Biosens. Bioelectron.*, 2024, **261**, 116509.

145 J. S. Nah, S. C. Barman, A. Zahed, M. Sharifuzzaman, H. Yoon, C. Park, S. Yoon, S. Zhang and J. Y. Park, *Sens. Actuators, B*, 2020, **329**, 129206.
146 S. Zhu, D. Wang, M. Li, C. Zhou, D. Yu and Y. Lin, *J. Mater. Chem. B*, 2022, **10**, 2113–2125.
147 B. Gürbüz and F. Ciftci, *Chem. Eng. J.*, 2024, **489**, 151230.
148 B. Ryplida and S. Y. Park, *Sens. Actuators, B*, 2023, **394**, 134363.
149 S. Hroncekova, T. Bertok, M. Hires, E. Jane, L. Lorencova, A. Vikartovska, A. Tanvir, P. Kasak and J. Tkac, *Processes*, 2020, **8**, 580.
150 Q. Zhang, H. Zhang, J. Liang, X. Zhao, B. Li, J. Zang, L. Gao, Z. Zhang and C. Xue, *J. Mater. Chem. C*, 2023, **11**, 15638–15648.
151 Z. Shi, C. Dai, P. Deng, X. Li, Y. Wu, J. Lv, C. Xiong, Y. Shuai, F. Zhang, D. Wang, H. Liang, Y. He, Q. Chen, Y. Lu and Q. Liu, *Sens. Actuators, B*, 2023, **383**, 133598.
152 Z. Chen, Y. Liu, W. Yu, S. Liu and Y. Huang, *ACS Appl. Nano Mater.*, 2025, **8**(11), 5602–5610.
153 X. Zheng, D. Zhou, Z. Liu, X. Hong, C. Li, S. Ge and W. Cao, *Small*, 2024, **20**, 2310032.
154 X. Xu, Y. Chen, P. He, S. Wang, K. Ling, L. Liu, P. Lei, X. Huang, H. Zhao, J. Cao and J. Yang, *Nano Res.*, 2021, **14**, 2875–2883.
155 S. Sharma, A. Chhetry, M. Sharifuzzaman, H. Yoon and J. Y. Park, *ACS Appl. Mater. Interfaces*, 2020, **12**, 22212–22224.
156 Y. Feng, H. Liu, W. Zhu, L. Guan, X. Yang, A. Zvyagin, Y. Zhao, C. Shen, B. Yang and Q. Lin, *Adv. Funct. Mater.*, 2021, **31**(46), 2105264.
157 H. L. Chia, C. A.-O. Mayorga-Martinez, N. A.-O. Antonatos, Z. A.-O. Sofer, J. J. Gonzalez-Julian, R. A.-O. Webster and M. A.-O. Pumera, *Anal. Chem.*, 2020, **92**(3), 2452–2459.
158 T. Cui, Y. Qiao, D. Li, X. Huang, L. Yang, A. Yan, Z. Chen, J. Xu, X. Tan, J. Jian, Z. Li, S. Ji, H. Liu, Y. Yang, X. Zhang and T.-L. Ren, *Chem. Eng. J.*, 2023, **455**, 140690.
159 M. Sang, S. Liu, W. Li, S. Wang, J. Li, J. Li, S. Xuan and X. Gong, *Composites, Part A*, 2022, **153**, 106727.
160 X. Li, Z. An, Y. Lu, J. Shan, H. Xing, G. Liu, Z. Shi, Y. He, Q. Chen, R. P. S. Han, D. Wang, J. Jiang, F. Zhang and Q. Liu, *Adv. Mater. Technol.*, 2022, **7**, 2100872.
161 Q. Yu, J. Jiang, C. Su, Y. Huang, N. Chen and H. Shao, *Text. Res. J.*, 2022, **92**, 810–824.
162 Q. Wang, X. Pan, C. Lin, H. Gao, S. Cao, Y. Ni and X. Ma, *Chem. Eng. J.*, 2020, **401**, 126129.
163 H. Su, K. A. S. Usman, A. Nilghaz, Y. Bu, K. Tang, L. Dai, D. Liu, J. M. Razal, W. Lei and J. Tian, *Device*, 2024, **2**(5), 100356.
164 T. Kang, W. Ma, Y. Guo, J. Zhou, Y. Zhang, T. Ji, W. Zhang and W. Gong, *Nano Energy*, 2023, **110**, 108359.
165 A. Hazarika, B. K. Deka, J. Seo, H. E. Jeong, Y.-B. Park and H. W. Park, *Nano Energy*, 2021, **86**, 106042.
166 F. Chen, H. Deng, G. Li, X. Li, J. Pan, T. Liu and T. Gong, *Chem. Eng. J.*, 2024, **489**, 151221.
167 K. Ji, Z. Liang, P. Wang, Z. Li, Q. Ma and X. Su, *Chem. Eng. J.*, 2024, **495**, 153598.
168 Y. Zhang, L. Wang, L. Zhao, K. Wang, Y. Zheng, Z. Yuan, D. Wang, X. Fu, G. Shen and W. Han, *Adv. Mater.*, 2021, **33**, 2007890.
169 A. M. Amani, L. Tayebi, M. Abbasi, A. Vaez, H. Kamyab, S. Chelliapan and E. Vafa, *ACS Omega*, 2023, **9**, 3123–3142.
170 F. Cao, Y. Zhang, H. Wang, K. Khan, A. K. Tareen, W. Qian, H. Zhang and H. Ågren, *Adv. Mater.*, 2022, **34**, 2107554.
171 R. A. Soomro, P. Zhang, B. Fan, Y. Wei and B. Xu, *Nano-Micro Lett.*, 2023, **15**, 108.
172 J. Jiang, S. Bai, J. Zou, S. Liu, J.-P. Hsu, N. Li, G. Zhu, Z. Zhuang, Q. Kang and Y. Zhang, *Nano Res.*, 2022, **15**, 6551–6567.
173 Y. Han, J. Hu, X. Liu and F. Liu, *Materials*, 2025, **18**, 3576.
174 H. Huang, R. Jiang, Y. Feng, H. Ouyang, N. Zhou, X. Zhang and Y. Wei, *Nanoscale*, 2020, **12**, 1325–1338.
175 M. Mozafari and M. Soroush, *Mater. Adv.*, 2021, **2**, 7277–7307.
176 F. Morshedi Dehaghi, M. Aberoumand and U. Sundararaj, *Molecules*, 2025, **30**, 1955.
177 S. Iravani, A. Zarepour, E. Nazarzadeh Zare, P. Makvandi, A. Khosravi and A. Zarrabi, *FlatChem*, 2024, **48**, 100759.
178 E. Mostafavi and S. Iravani, *Nano-Micro Lett.*, 2022, **14**, 130.
179 A. Zarepour, S. Ahmadi, N. Rabiee, A. Zarrabi and S. Iravani, *Nano-Micro Lett.*, 2023, **15**, 100.
180 F. Mohajer, G. M. Ziarani, A. Badiei, S. Iravani and R. S. Varma, *Nanomaterials*, 2023, **13**, 345.
181 A. Rasheed, S. Ajmal, P. Wang and S. G. Lee, *Appl. Mater. Today*, 2024, **39**, 102270.
182 A. Lipatov, A. Goad, M. J. Loes, N. S. Vorobeva, J. Abourahma, Y. Gogotsi and A. Sinitskii, *Matter*, 2021, **4**, 1413–1427.
183 Y. I. Jhon and J. H. Lee, *Comput. Mater. Sci.*, 2023, **227**, 112268.
184 Y. Liu, Q. Tang, M. Xu, J. Ren, C. Guo, C. Chen, W. Geng, W. Lei, X. Zhao and D. Liu, *Chem. Eng. J.*, 2023, **468**, 143439.
185 S. Tian, K. Zhou, C.-Q. Huang, C. Qian, Z. Gao and Y. Liu, *Extreme Mechanics Letters*, 2022, **57**, 101921.
186 X. Li, Y. Lu and Q. Liu, *Talanta*, 2021, **235**, 122726.
187 J. Yoon, M. Shin, J. Lim, J.-Y. Lee and J.-W. Choi, *Biosensors*, 2020, **10**, 185.
188 D. Lu, H. Zhao, X. Zhang, Y. Chen and L. Feng, *Biosensors*, 2022, **12**, 820.
189 S. Alwarappan, N. Nesakumar, D. Sun, T. Y. Hu and C.-Z. Li, *Biosens. Bioelectron.*, 2022, **205**, 113943.
190 V. Kedambaimoole, K. Harsh, K. Rajanna, P. Sen, M. Nayak and S. Kumar, *Mater. Adv.*, 2022, **3**, 3784–3808.
191 K. Xie, J. Wang, S. Xu, W. Hao, L. Zhao, L. Huang and Z. Wei, *Mater. Des.*, 2023, **228**, 111867.
192 Q. Wang, N. Han, Z. Shen, X. Li, Z. Chen, Y. Cao, W. Si, F. Wang, B.-J. Ni and V. K. Thakur, *Nano Mater. Sci.*, 2023, **5**, 39–52.
193 A. M. Jastrzębska, A. Szuplewska, T. Wojciechowski, M. Chudy, W. Ziemkowska, L. Chlubny, A. Rozmysłowska and A. Olszyna, *J. Hazard. Mater.*, 2017, **339**, 1–8.
194 G. P. Lim, C. F. Soon, N. L. Ma, M. Morsin, N. Nayan, M. K. Ahmad and K. S. Tee, *Environ. Res.*, 2021, **201**, 111592.

195 S. Sagadevan and W.-C. Oh, *J. Drug Delivery Sci. Technol.*, 2023, **85**, 104569.
196 T. R. Dmytriv and V. I. Lushchak, *Chem. Rec.*, 2024, **24**, e202300338.
197 V. G. Gayathri, B. Richard, J. T. Chacko, J. Bayry and P. A. Rasheed, *J. Mater. Chem. B*, 2025, **13**, 1212–1228.
198 T. Li, W. Qiang and B. Lei, *Nanoscale*, 2025, **17**, 4854–4891.
199 T. Hussain, I. Chandio, A. Ali, A. Hyder, A. A. Memon, J. Yang and K. H. Thebo, *Nanoscale*, 2024, **16**, 17723–17760.
200 S. Iravani, A. Khosravi, E. Nazarzadeh Zare, R. S. Varma, A. Zarrabi and P. Makvandi, *RSC Adv.*, 2024, **14**, 36835–36851.